UNITED NATIONS EDUCATIONAL, SCIENTIFIC AND CULTURAL ORGANIZATION
INTERNATIONAL ATOMIC ENERGY AGENCY
INTERNATIONAL CENTRE FOR THEORETICAL PHYSICS
I.C.T.P., P.O. BOX 586, 34100 TRIESTE, ITALY, CABLE: CENTRATOM TRIESTE

SMR.998c - 10

Research Workshop on Condensed Matter Physics
30 June - 22 August 1997

MINIWORKSHOP ON PATTERN FORMATION AND SPATIO-TEMPORAL CHAOS 28 JULY - 8 AUGUST 1997

"Chemical oscillating reactions and the principles of open spatial reactors"

"The Turing and Hopf instabilities and their interactions in the CIMA reaction"

"Three dimensional aspects and effects of parameter ramps on pattern selections"

"Beyond standard growth dynamics of Turing patterns: Interaction between Turing and stationary uniform instabilities"

P. DE KEPPER
Centre National de la Recherche Scientifique
Centre de Recherche Paul Pascal
Avenue A. Schweitzer
Bordeaux
33600 Pessac
FRANCE

These are preliminary lecture notes, intended only for distribution to participants.

Physica A 188 (1992) 1–16
North-Holland

PHYSICA A

Stationary Turing patterns versus time-dependent structures in the chlorite–iodide–malonic acid reaction

J.J. Perraud, K. Agladze, E. Dulos and P. De Kepper

Centre de Recherche Paul Pascal/CNRS, Université Bordeaux I, Av. A. Schweitzer, 33600 Pessac, France

The standing concentration patterns recently discovered in open gel-filled reactors, with the chlorite–iodide–malonic acid (CIMA) oscillating reaction in the presence of starch, were ascribed to a Turing-type reaction–diffusion symmetry breaking instability. Here we extend the investigations to other regions of parameters, with a particular emphasis to the role played by the chemical nature of the gel matrix and by the starch concentration on the onset of stationary patterns. Stationary Turing patterns are shown to develop in gel-free systems. Transitions between stationary Turing structures and wave patterns are presented. The first evidence of an anti-symmetric "homogeneous" wave source is presented.

1. Introduction

The first clear evidence, in a single-phase system, of the stationary concentration patterns predicted by Turing, in 1952 [1], was made in our laboratory in December 1989 [2, 3]. This long sought nonequilibrium chemical structure [4, 5] was obtained by operating the chlorite–iodide–malonic acid (CIMA) reaction [6, 7] in an open spatial reactor. This discovery sets chemical systems again in the main stream of the most advanced problems of nonlinear physics and has revived theoretical studies on Turing patterns [8–12] with special emphasis on pattern selection in three-dimensional systems [9, 10] and on the role played by the technically unavoidable constraint gradients in the spatial mode selection processes [8]. The initial experimental ascertainment of Turing pattern was rapidly confirmed in other laboratories [13] and new properties of these standing spatial structures were investigated [13–16].

In this report, we summarize some of our previous observations, enlarge the scope of investigation, and describe a number of undocumented phenomena. We shall, in particular, address problems such as those risen by the tridimensionality of the patterns, by the possible interaction with the gel-matrix, and the actual role of starch. Finally we will focus on a new type of

"homogeneous" wave source that we have dubbed "*chemical flip-flop*". But first, let us introduce the basic principles of the open spatial reactors used in Turing patterns experiments.

2. Experimental materials

2.1. Principles of the open spatial reactors

Different geometries (rectangular [2], annular [3], disc [13, 14] capillary tube [16]) of open spatial reactors have been used in experiments on Turing structures, but they are all based on the same principles. Generally, the reactor proper is a block of hydrogel (fig. 1) inside which different reactants diffuse from two opposing sides in contact with the contents of two stirred reservoirs (i.e. reservoir I and II in fig. 1) of reagents permanently renewed; the other sides are usually impermeable or periodic boundaries. The hydrogel medium is primarily used to avoid any parasitic convective motion to develop in the reaction fluid, and yet to allow small soluble species to diffuse almost freely. The gel matrix should be chemically inert and transparent. Two chemically different hydrogels were used in the experiments reported below, a 5% polyacrylamide gel characterized by an average pore size of 80 Å and a 2% agarose gel with an average pore size of 5000 Å. Both gels are loaded with a soluble starch, a color indicator of the reaction. Soluble starch, or amylose, is a large polysaccharide with a molecular weight generally above 200 000 Daltons. In our experiments the iodine color indicator is not pure starch but Thiodène – a cold water soluble material from PROLABO France – made of 7% specially treated amylose and 93% urea [15]. Note that after preparation of the Thiodène loaded gel, the excess urea is rapidly washed out, while the large

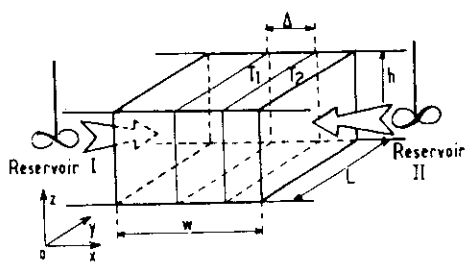

Fig. 1. Basic principles of open spatial reactors. Reservoirs I and II are constantly fed with fresh solutions of reagents. Stirring insures that concentrations are uniform along the feed surfaces (for details see text).

amylose molecule remains totally or partially immobilized in the gel matrices. As explained later, starch is in fact much more than the color indicator of the reaction. Some experiments were performed in capillary tubes only filled with solutions of starch (i.e. without gel) [16]. In this case, the reaction cell is separated from the feed tanks by two membranes which let small solvated species diffuse across but not starch.

Inside the gel, in the absence of any spatial instability, a composition gradient naturally settles perpendicular to the feed surfaces with iso-concentration planes parallel to these surfaces. For appropriate boundary feed concentrations, a region of Turing instability can develop between two critical planes (T_1 and T_2) [17, 18] parallel to the feed surfaces (fig. 1). The wavelength λ of the patterns does not depend on any geometric dimension, but only on the kinetic and the diffusion constants. Thus, depending on how λ compares to the other dimensions (Δ the distance between the critical Turing planes, the length L, and the height h), one-, two- or three-dimensional patterns can develop.

Two main directions of observations have been used in these reactors: (i) One in the Oz (fig. 1) direction, parallel to the feed surfaces, allows for an easy count of the number of structured planes piling in the direction of the composition gradients [2, 3, 16]. (ii) The other in the Ox direction, perpendicular to the feed surfaces, allows for a more dramatic view of the spatial symmetry breaking properties of the patterns [13, 14]. The monitoring is usually made by a video CCD camera and pictures are ultimately intensified by image-processing.

2.2. The reaction

The chlorite–iodide–malonic acid (CIMA) reaction is a redox reaction characterized by positive feedbacks due to both iodine autocatalysis and iodide substrate inhibition kinetics [19, 20]. In a continuous well-stirred tank-reactor (CSTR), the reaction exhibits two quite different steady states, one characterized by high iodide and high iodine concentrations (HI), the other by very low iodide concentration (LI). These states are the continuations of the sole steady states observed when feed concentrations have respectively large excess reducer (iodide) and oxidant (chlorite) [19, 20]. In the presence of starch, the HI state colors in dark blue due to the formation of a reversible starch–triiodide complex [21], while the LI state remains pale yellow. At low malonic acid concentrations, the reaction can exhibit bistability between the HI and LI states, while for large enough malonic acid concentrations sustained oscillations between these two states are observed [20]. Detailed mechanistic studies of the reaction can be found in refs. [7, 19].

3. Experimental results

3.1. Symmetry breaking and non-symmetry breaking patterns

The initial Turing experiments were performed in thick rectangular strips where $\lambda < h < w \ll L$ ($h = 1$ mm, $w = 3$ mm, $L = 20$ mm) with observation made in the Oz direction (fig. 1). In the focal plane of the camera, patterns appeared either as clear and dark bands parallel to the feed surfaces or as rows of clear dots in a darker background. The latter pattern breaks the boundary feed symmetry.

In all the experiments presented in this paper, the reagents are distributed in the reservoirs in such way that each mixture is separately nonreactive, so that boundary feed compositions are well defined. The reaction only occurs inside the gel where all major species are in significant concentration. The values of the chemical parameter $[X]_0^{I,(II)}$ correspond to the concentration of species X in reservoir I or II. Chlorite is only introduced in reservoir II, in stoichiometry excess. As a consequence, the LI state is favored along this reservoir and the reaction medium remains colorless on this edge. Conversely, iodide is in excess in reservoir I and the dark-blue HI state is always observed next to this reservoir. A waterjacket maintains the whole system at constant temperature.

A series of experimentally observed spatial patterns are gathered in fig. 2. They were obtained by a gradual increase of the chlorite concentration in reservoir II. At low $[ClO_2^-]_0^{II}$, a single sharp color change develops parallel to the feed boundaries, forming a stable chemical front between the two edges of the strip. This trivial concentration pattern corresponds to a sharp switch between the dark HI and the clear LI states, which dominate respectively at one and the other side of the strip. On increasing $[ClO_2^-]_0^{II}$, a pattern of two alternating dark and clear bands develops also parallel to the feed boundaries (fig. 2a). This stationary structure is similar to the structure observed in the Couette flow reactor with analogous asymmetric boundary conditions [22]. At slightly higher values of the control parameter, an additional faint dark band develops parallel to the previous one. On further increasing $[ClO_2^-]_0^{II}$, a completely new type of pattern develops. The latter continuous parallel bands break into rows of clear spots embedded in a light blue region (fig. 2b). The number of rows of spots which develop parallel to the feed surfaces depends on the value of the control parameter (fig. 2b, fig. 2c). Up to four rows of spots have been observed [3]. At still higher chlorite feed concentration, the spot pattern eventually disappears and parallel band patterns are recovered (fig. 2d).

The spot pattern spontaneously breaks the boundary feed symmetry of the system. Within the present experimental accuracy, these patterns appear and

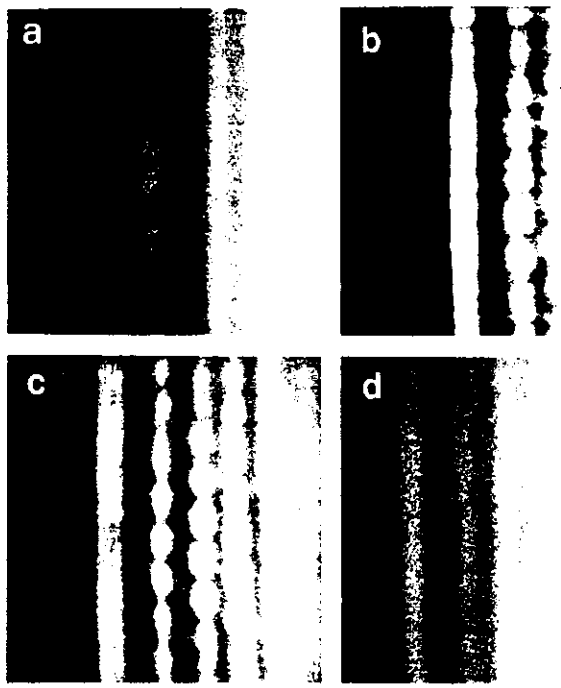

Fig. 2. Set of spatial pattern observed in the thick strip reactor filled with polyacrylamide. Boundary feed composition: $[I^-]_0^{I,II} = 1.7 \times 10^{-1}$ M; $[CH_2(COOH)_2]_0^{I} = 6.7 \times 10^{-1}$ M; $[H_2SO_4]_0^{I} = 10^{-2}$ M; $[NaOH]_0^{II} = 3 \times 10^{-1}$ M; with: (a) two bands pattern, parallel to the feed boundaries, $[ClO_2^-]_0^{II} = 1.33 \times 10^{-2}$ M; (b) and (c) spot patterns breaking the boundary feed symmetry $[ClO_2^-]_0^{II} = 2 \times 10^{-2}$ M, $[ClO_2^-]_0^{II} = 2.4 \times 10^{-2}$ M respectively, temperature 5°C; (d) multiple band pattern $[ClO_2^-]_0^{II} = 2.8 \times 10^{-2}$ M. View field 1.6 mm × 1.6 mm.

disappear reproducibly, without hysteresis, as a function of the control parameters. Though there are some irregularities in the intensity modulations of patterns, they usually have well defined wavelength λ, typically $\lambda \simeq 0.2$ mm, as for the patterns in figs. 2b and 2c. This wavelength is smaller than all the dimensions of the reactor.

Taking into account that the characteristic focal depth of our lens is about 0.5 mm, the pictures correspond to projections of an actually three-dimensional structure. When the spot pattern clearly develops over three (fig. 2c) or more lines, the top view corresponds to an hexagonal packing. Different types of three-dimensional organizations [10, 11], such as prismatic columns or body centered cubic (bcc), could be consistent with this projection. Observations

made under different angles (fig. 3), usually show a beady structure that is more consistent with a bcc organization.

However, the recognition of the exact type of lattice packing is made difficult by the development of many crystalline defects [8]. The transverse composition gradient is a major source of defects, because the different iso-concentration planes can correspond to patterns with different wavelengths and even to different stable spatial modes [12]. The interaction between planes of different spatial modes could stabilize otherwise unstable modes, like mixed modes [13, 14].

Projections of the tridimensional pattern arrangements can also be at the origin of artefacts. For example, in thick reactors, when a very high acid concentration gradient is set between the two surfaces, two quite different types of patterns (fig. 4a and 4b) can be simultaneously observed from the Oz

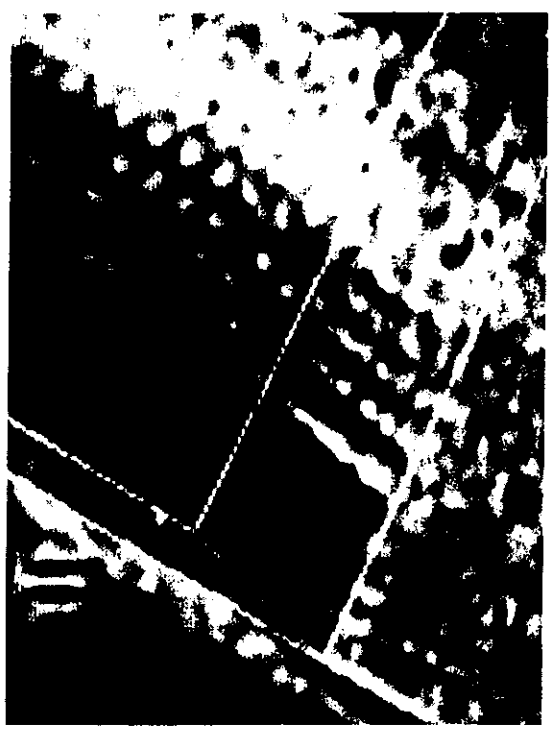

Fig. 3. Perspective view of the 3-D spot Turing pattern in a thick strop reactor ($h = 1$ mm, $w = 3$ mm, $L = 20$ mm). Partial view, the edges of the gel reactor are underlined.

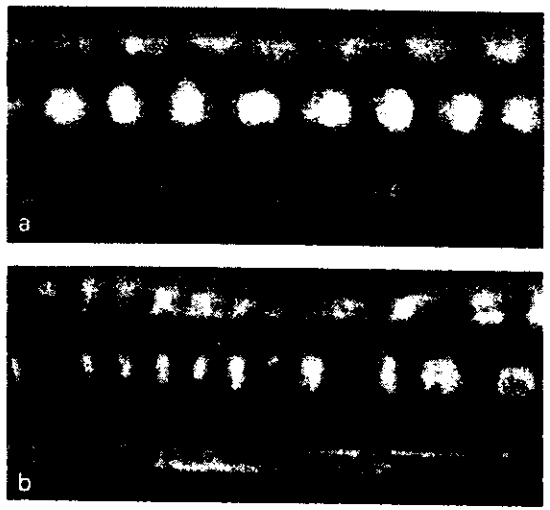

Fig. 4. "Two wavelengths mixed patterns" (a) and (b) are observed along the same thick polyacrylamide gel strip reactor. (a) Large wavelength patterns; (b) small wavelength patterns, on the left of the picture. Boundary feed composition: $[I^-]_0^{I,II} = 1.7 \times 10^{-3}$ M, $[CH_2(COOH)_2]_0^I = 8.33 \times 10^{-1}$ M, $[H_2SO_4]_0^I = 16 \times 10^{-2}$ M, $[ClO_2]_0^{II} = 2.4 \times 10^{-2}$ M, $[NaOH]_0^{II} = 3 \times 10^{-1}$ M; temperature 5°C.

direction (fig. 1). Patterns of two different wavelengths seem to coexist, in randomly distributed patches, along rows at the same distance from the feed surfaces. Similar observations were also reported by H.L. Swinney during this conference. Measurements of the large to small wavelengths ratio of such "mixed wavelength structures" usually give values close to 1.7 or 2, as in fig. 4. However, experiments with the same feed concentrations but operated in reactors where the view could be made in the Ox direction (fig. 1) only showed patterns with the largest wavelength. The small wavelength is an illusion due to side projections of planar arrangements of centered hexagon patterns. From simple geometric considerations, one can determine that the planar orthogonal projections of an hexagon point lattice, on axes respectively parallel and perpendicular to the diagonal of the hexagons, give linear arrays with a ratio of distances equal to $\sqrt{3} = 1.73$. This value is exactly in the range of wavelength ratio often found in the "mixed wavelength structures". Nevertheless, in real systems, the actual result of such type of projections would greatly depend on the concentration profiles of the individual large spots. To support the above interpretation with projections of real intensity profiles, we have created and artifical image, fig. 5, resulting from the addition of two images 4a shifted by

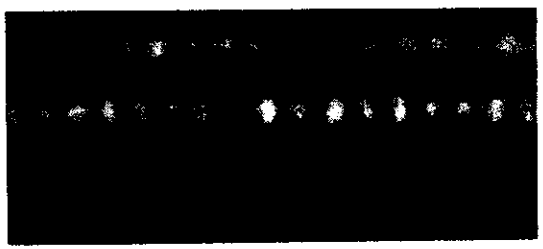

Fig. 5. Artefact image produced by the addition of two images identical to fig. 4a but one shifted half a wavelength relative to the other.

half a wavelength. The result is qualitatively identical to fig. 4b, small elongated spots are clearly seen, with a wavelength half the initial one.

Beyond the spot patterns, band patterns are often observed (figs. 2a and 2d). The origin of these band patterns is still unclear. They could be related, either to the gradient induced structures, as discussed by Arneodo and Elezgaray [23] or to another mode of the Turing instability, namely the periodic sheet patterns also predicted to develop in three dimensional reaction–diffusion systems [9, 10].

3.2. *The role of the gel matrix*

In order to determine the effective role of gels in the development of Turing patterns, a set of experiments was performed in a capillary tube reactor, 0.2 mm diameter and $w = 3$ mm, equal to the distance between the feed surfaces in the former thick strip reactor. The capillary reactor is filled either with polyacrylamide or with agarose gels. The advantage of this small reactor is that it makes possible experiments in gel-free solutions, without convection. The tube is closed at both ends by a dialysis membrane, 0.12 mm thick, able to retain starch and let the other species freely diffuse across. The feed compositions are similar to those used with the thick strip reactor. All experiments were performed with approximately the same high concentration of starch. Fig. 6a shows a typical spatial pattern obtained when the capillary tube was filled with a polycrylamide gel. The pattern is like that observed, with the same angle of view, in much larger spatial reactors (see fig. 2c). Beyond the first clear band on the right, a spot pattern, which breaks the boundary feed symmetry, develops over several rows. The apparent pattern is two-dimensional with a wavelength, $\lambda = 0.13 \pm 0.01$ mm, slightly less than the diameter of the tube. Figs. 6b and 6c present the results of similar experiments performed in an

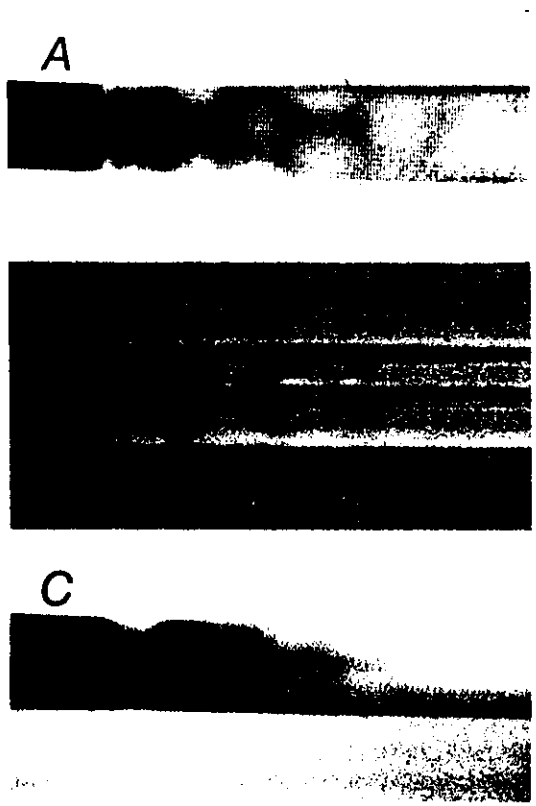

Fig. 6. Standing Turing patterns observed in the capillary tube reactor. (a) Reactor filled with a 5% polyacrylamide gel loaded with Thiodène: 130g/ℓ. (b) Reactor filled with a 1.2% agarose gel loaded with Thiodène: 80g/ℓ. (c) Gel-free reactor containing a solution of Thiodène: 100g/ℓ. The starch solution is maintained by membranes at each end of the tube. Boundary feed conditions: $[I^-]_0^{II} = 2.5 \times 10^{-3}$ M, $[CH_2(COOH)_2]_0^{I} = 8.15 \times 10^{-3}$ M, $[H_2SO_4]_0^{I} = 9.3 \times 10^{-3}$ M, $[ClO_2^-]_0^{II} = 2.4 \times 10^{-2}$ M, $[NaOH]_0^{II} = 2 \times 10^{-3}$ M, temperature 5°C.

agarose gel and in a gel-free starch solution, respectively. The spot patterns, though less outspread, are clearly observable in both cases. As previously, the patterns do not develop with the simple axial symmetry of the tube, even though in the latter two experiments the wavelength is $\lambda = 0.2$ mm, exactly the diameter of the tube. These results clearly show that Turing structures are not linked to any particular property of the polyacrylamide gel. However, as illustrated by the differences between the patterns in figs. 6a and 6b, for

identical feed conditions and starch concentrations, patterns develop over a more reduced number of rows in agarose than in polyacrylamide. In any case, as shown in fig. 6c, gels are not crucial for the onset of Turing patterns in the CIMA reaction.

3.3. The role of starch

Except in very particular cases [24, 25], Turing structures call for important differences in the mobility of reactive species [1, 4], but in plain aqueous solutions, all the small halogen compounds involved in the CIMA reaction have approximately the same value of diffusion coefficients. Always present in the reaction medium, the soluble starch is the only large molecule with a very different mobility and able to interact with the reactive halogen compounds. As mentioned above, the starch used in our experiments is essentially immobilized in the gels, and even in plain solution, its diffusion coefficient is more than an order of magnitude less than that of the other species.

It was suggested [26] and formally calculated by Lengyel and Epstein [27], on the basis of a skeleton kinetic mechanism of the reaction, that the reversible adsorption of iodide and iodine on the immobile starch leads to a decrease of the effective diffusion of these species. Note that iodide is the species controlling the positive feedback loop of the reaction. On the other hand, the diffusion of chlorite, the species acting as an inhibitor would remain essentially unchanged [26, 27]. Low diffusivity of the positive feedback species together with relatively high diffusivity of the negative feedback species are an essential feature of models leading to Turing patterns [1, 2, 9–12, 26, 28, 29].

Experiments with different starch concentrations were performed in the different gels and in gel-free systems. In polyacrylamide-filled reactors, the decrease of the Thiodène concentration [15]. From 100 g/ℓ to 2.5 g/ℓ, for the same feed concentrations as for the experiments of fig. 2c, essentially leads to a decrease, from four to two, in the number of detectable rows of standing dot pattern and a slight increase of the wavelength of 15%. Below this lowest concentration, patterns become very difficult to detect mainly because of the natural color fading with the decrease of the color indicator concentration. It seems that in polyacrylamide gels, standing Turing patterns can be obtained even in the absence of starch [30]. In agarose-filled gel-reactors, the decrease of starch concentration generally leads to a transition from standing structures to travelling wave patterns. In the rectangular strip reactor, when gels with decreasing starch concentrations are used, periodic front oscillations are observed, at the location of the previous standing patterns, below a critical starch concentration value. This critical value depends on other constraint values. The front oscillations usually organize in wavetrains. A snapshot of such a wave

Fig. 7. Travelling wave pattern observed in a 2% agarose gel strip reactor loaded with 6g/ℓ Thiodène solution. All feed concentrations are as in fig. 6. The bar inside the picture represents 1 mm. The spearhead shaped wave train travels from right to left.

train is presented in fig. 7. The wave pattern is produced by the periodic appearance of two sharp clear planar fronts travelling "toward" each other and stopping simultaneously at a fixed distance from the feed surfaces. The two fronts do not collide like trigger waves in the Belousov–Zhabotinsky reaction [31]; at the collision location a permanent dark region parallel to the feed surfaces is left. The synchronous motion of these pairs of waves forms spearhead patterns moving parallel to the feed boundary, as shown in fig. 7. At the present time, it is difficult to ascertain if these waves are of trigger-type or if they are just sustained phase waves [32]. Waves can either start from the ends of the gel strip, where some ill-defined feed conditions can occur or from defects in the gel (i.e. notches, cracks, dust particles). Waves form and develop symmetrically around these defect mediated pacemakers. In the experiment shown in fig. 7, the period of oscillations is 26 s. Similar experiments were also performed in the gel-free capillary reactor and, as in the case of agarose gel, the region of standing spot pattern is changed into a region of pulsating fronts, below a critical value of starch concentration.

Note that standing concentration patterns are favored when a polyacrylamide gel is used. In fact, we have never observed any oscillatory dynamics for any feed composition when polyacrylamide gels were used. Thus, the polyacrylamide matrix seems to be capable to play a role similar to that of starch. This particular property limits investigation to transitions between

different standing patterns. As we shall see below, a rich variety of spatio-temporal behaviors can be obtained with the CIMA reaction when operated in other more "neutral" gels where the transitions between stationary and non-stationary patterns can be investigated. Note that agarose gel and also silica gel [33] give results very similar to those found in plain water solutions.

4. The chemical 'flip-flop'

In order to analyze the possible sequence of spatio-temporal states extending from standing Turing structures to simple wave patterns, we have started a systematic exploration of the parameter space between these two states. Experiments were performed in a relatively thin (0.3 mm) rectangular agarose gel strip. Thinner strips were used in order to minimize the possible artefacts due to the development of 3D waves. Among the wealth of very complex dynamical states encountered, some of them reminiscent of turbulence [34], we report on the observation of unusual wave sources. In contrast to the wave sources mentioned above, this new one is not linked to any particular feed inhomogeneity or heterogeneity in the medium. As explained later, this source can appear and disappear at different positions and occasionally slowly drift. This wave source has the aspect of an isolated Turing-type spot, a clear dot in a slightly darker immediate surrounding (fig. 8). Starting from this clear spot, wavetrains propagate away on both sides along a thin dark band parallel to the feed surfaces (fig. 8a). The local period of oscillations is in this case 32 s. At a distance from the source, the wavetrains have exactly the same characteristics as those discussed earlier (fig. 7). However, amazingly the left and right waves are not emitted synchronously by the pacemaker. This is illustrated in figs. 8b and 8c where the two snapshots are separated by half a period. The two pictures are the mirror images of each other. A closer look to the dynamics of the source spot, reveals that, in fact, the bright core flips from one side to the other of a narrow region which remains essentially invariant in time.

Fig. 9 gathers three sets of light intensity profiles in the *Oy* and *Ox* directions. In the *Oy* direction, the set of curves is taken along a line 0.1 mm above the permanent dark line acting as a trail for the waves (fig. 9a). The four intensity curves are taken at quarter-period intervals. All the profiles cross in a same small region and no oscillation occurs over that place; notice that the curves pair two by two as in a mirror. The two sharp high intensity peaks at $t = 8$ s and $t = 24$ s set the limit between which the bright "Turing spot" source flips back and forth and emits a pair of clear waves either on the right or on the left. The two peaks are 0.3 mm apart. In the *Ox* direction, a first set of profiles (fig. 9b) is taken at some distance (0.5 mm) from the source; it shows that the

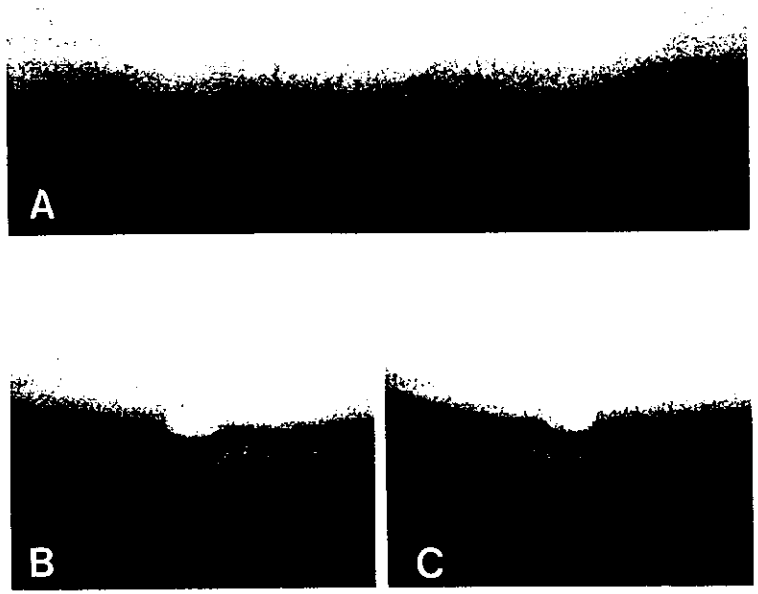

Fig. 8. Chemical flip-flop: (a) Snapshot of wave source and of the surrounding wave trains. The bar inside the picture represents one millimeter. (b) and (c) snapshots of the wave source taken at 16 s time intervals. Notice that (b) and (a) are mirror images. Waves are produced anti-symmetrically. Boundary feed compositions: $[I^-]_0^{I,II} = 2.5 \times 10^{-3}$ M, $[CH_2(COOH)_2]_0^I = 10^{-2}$ M, $[CH_3COOH]_0^I = 2.2$ M, $[ClO_2^-]_0^{II} = 2.4 \times 10^{-2}$ M, $[NaOH]_0^{II} = 3 \times 10^{-1}$ M; temperature 3°C.

oscillatory domain only extends over a narrow region (0.4 mm wide) on both sides of the permanent dark line. The permanent dark line corresponds to the zone of minimum amplitude oscillations in the middle. The last set of profiles, also in the *Ox* direction, is taken exactly through the motionless region of fig. 9a. Astonishingly, these profiles show that there is no oscillation anywhere along this line; it seems to correspond to a stationary region around which a bascule phenomenon develops. We have dubbed this undocumented wave source a "*chemical flip-flop*". The flip-flop sources can appear or disappear

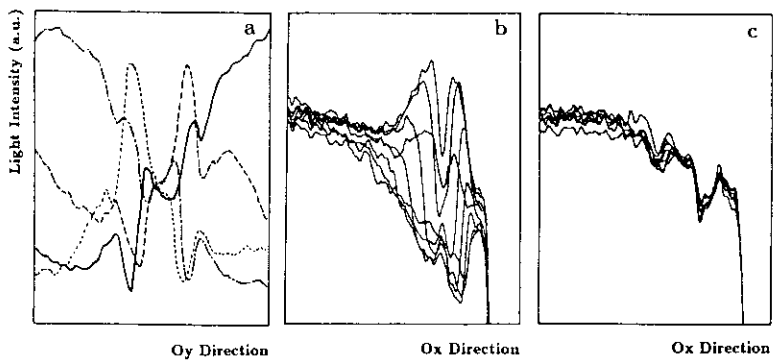

Fig. 9. Sets of light intensity profiles taken across the Ox and Oy directions in fig. 9b. (a) In the Oy direction, profile at time $t = 0$ – – – –; $t = 8$ s – – – –; $t = 16$ s ———; $t = 24$ S -------. (b) In the Ox direction at 0.5 mm from the source. (c) In the Ox direction through the source (for details see text). In (b) and (c) 8 profiles are taken at 4 s time intervals.

reversibly as a function of the control parameter, from the simple wave state. Yet, they do not always reappear at the same location. Very often, the sources do not stay at the place where they are formed, but very slowly drift parallel to the feed surfaces. Eventually, a flip-flop stops at some positions which sometimes clearly match with the vicinity of defects in the gel. The phenomenon does not depend on the thickness of the medium, similar sources were obtained with 0.14 mm thick gels. As a matter of fact, the phenomenon seems to be effectively one-dimensional.

We know of no straightforward theoretical explanation that fits all the characteristics of our chemical flip-flops. Their existence seems to be linked to the vicinity, in the parameter space, of standing Turing patterns and they can develop spontaneously in an oscillating medium. Some similarities could be found with the echo-waves initially proposed by Krinsky [35, 36] as pacemakers in excitable tissues, but such echo-waves do not form spontaneously and need to be initiated by some particular symmetry breaking conditions. An other interesting type of 'homogeneous' wave source was proposed by Dewel and Borckmans [37]. Their approach, based on the notion of localized state, first introduced by Thual and Fauve [38], leads to symmetric and antisymmetric wave sources but as for echo-waves they need to be triggered by an initial perturbation. Clearly, our observations call for new theoretical investigations on the interaction of Turing and Hopf bifurcations, and models with more than two independent species might be necessary to account for the zoology of spatio-temporal behavior in real chemical systems.

Acknowledgements

We thank J. Boissonade, P. Borckmans, and G. Dewel, for fruitful discussions. This work is partly supported by Twinning contract #SC1-91-0706 of the EC Science Program.

References

[1] A.M. Turing, Philos. Trans. R. Soc. London B 327 (1952) 37.
[2] V. Castets, E. Dulos, J. Boissonade and P. De Kepper, Phys. Rev. Lett. 64 (1990) 2953.
[3] P. De Kepper, V. Castets, E. Dulos and J. Boissonade, Physica D 49 (1991) 161.
[4] G. Nicolis and I. Prigogine, Self-organization in Nonequilibrium Chemical Systems (Wiley, New York, 1977).
[5] H. Haken, Synergetics, an Introduction (Springer, Berlin 1977); Advanced Synergetics (Springer, Berlin, 1983).
[6] P. De Kepper, I.R. Epstein, K. Kustin and M. Orbán, J. Phys. Chem. 86 (1982) 170.
[7] I. Lengyel, G. Rabai and I.R. Epstein, J. Am. Chem. Soc. 112 (1990) 46066, I. Lengyel, G. Rabai and I.R. Epstein, J. Am. Chem. Soc. 112 (1990) 91046.
[8] J. Boissonade, V. Castets, E. Dulos and P. De Kepper, ISMN 97 (Birkhaüser, Basel, 1991) pp. 67–77.
[9] V. Dufiet and J. Boissonade, J. Chem. Phys. 96 (1992) 664; V. Dufiet and J. Boissonade, Physica A 188 (1992) 158, this Workshop.
[10] D. Walgraef, G. Dewel and P. Borckmans, Adv. Chem. Phys. XLIX (1982) 311; G. Dewel and P. Borckmans, in: Patterns, Defects, and Materials Instabilities, D. Walgraef and N. Ghoniem, eds., NATO Adv. Stud. (Kluwer, Dordrecht), in press.
[11] P. Borckmans, G. Dewel and A. De Wit, in: Seeds: Genesis of Natural and Artificial Forms, Biotechnology 90: International Symposia in Picardy-Le Biopole Vegetal Ed. 1990, pp. 62–71; A. De Wit, G. Dewel, P. Borckmans and D. Walgraef, preprint July 1991.
[12] P. Borckmans, A. De Wit and G. Dewel, Physica A 188 (1992) 137, this Workshop.
[13] Q. Ouyang and H.L. Swinney, Nature 352 (1991) 610.
[14] Q. Ouyang and H.L. Swinney, Chaos 1 (1991) 411.
[15] Z. Noszticzius, Q. Ouyang and W.D. McCormick, J. Am. Chem. Soc. (1992), in press.
[16] K. Agladze, E. Dulos and P. De Kepper, J. Phys. Chem. 96 (1992) 2400.
[17] M. Herschkowitz-Kaufman and G. Nicolis, J. Chem. Phys. 56 (1972) 1890; M. Herschkowitz-Kaufman, Bull. Math. Biol. 37 (1975) 585.
[18] J. Boissonade, J. Phys. (Paris) 49 (1988) 541.
[19] P. De Kepper, J. Boissonade and I.R. Epstein, J. Phys. Chem. 94 (1990) 6525.
[20] Q. Ouyang, V. Castets, J. Boissonade, J.C. Roux, P. De Kepper and H.L. Swinney, J. Chem. Phys. 95 (1991) 351; Q. Ouyang, Ph.D. Thesis (1989).
[21] C.L. Cronan and F. W. Schneider, J. Phys. Chem. 73 (1969) 3990; A. Cesáro, J.C. Benegas and D.R. Ripoli, J. Phys. Chem. 90 (1986) 2787.
[22] Q. Ouyang, J. Boissonade, J.C. Roux and P. De Kepper, Phys. Lett. A 134 (1989) 282.
[23] A. Arneodo and J. Elezgaray, Phys. Lett. A 143 (1990) 25; J. Elezgaray and A. Arneodo, J. Chem. Phys. 95 (1991) 323.
[24] J.E. Pearson and W. Horsthemke, J. Chem. Phys. 90 (1989) 1588.
[25] A. Arneodo, J. Elezgaray, J.E. Pearson and T. Russo, Physica D 49 (1991) 141.
[26] I. Lengyel and I.R. Epstein, Science 251 (1990) 650.
[27] I. Lengyel and I.R. Epstein, Proc. Nat. Sci. USA (1992), to appear.
[28] H. Meinhardt, Models of Biological Pattern Formation (Academic Press, New York, 1982).
[29] J.D. Murray, Mathematical Biology (Springer, Berlin, 1989).

[30] K.J. Lee, W.D. McCormick, Z. Noszticzius and H.L. Swinney, J. Chem. Phys. 96 (1992) 4048.
[31] A.N. Zaikin and A.M. Zhabotinsky, Nature 225 (1970) 535; A.M. Zhabotinsky, A.N. Zaikin, J. Theor. Biol. 40 (1973) 45.
[32] Y. Kuramoto, Chemical Oscillation, Waves and Turbulence (Springer, Berlin, 1984).
[33] K. Agladze, unpublished results.
[34] P. Manneville, Dissipative structures and weak turbulence, (Academic Press, New York, 1990).
[35] V.I. Krinsky, A.M. Pertsov and A.N. Reshetilov, Biophys. 10 (1972) 289.
[36] J.J. Tyson, Ann. New York Acad. Sci. 316 (1979) 279.
[37] G. Dewel and P. Borckmans, in: Solitons and Chaos, I. Antoniou and F. Lamber, eds., Research Reports in Physics (Springer, Berlin, 1991).
[38] O. Thual and S. Fauve, J. Phys. (Paris) 49 (1988) 1829.

Physica Scripta. Vol. T67, 43–50, 1996

Standard and Nonstandard Turing Patterns and Waves in the CIMA Reaction

B. Rudovics, E. Dulos and P. De Kepper

Center de Recherche Paul Pascal, Avenue Schweitzer, Université de Bordeaux I, 33600 Pessac, France

Received January 25, 1996; accepted April 22, 1996

Abstract

We describe experimental evidence of stable triangular and hexagon-band mixed mode nonstandard patterns, in a three-dimensional chemical reaction–diffusion system with steep gradients of chemical constraints. These gradients confine the structures in a more or less thick stratum of the system. At onset, patterns develop in monolayers which approximate two-dimensional systems; but beyond onset, three-dimensional aspects have to be considered. We show that the nonstandard pattern symmetries result from the coupling of standard hexagonal and striped pattern modes which develop at adjacent positions, due to the differences in parameter values along the direction of the gradients.

We evidence a Turing–Hopf codimension-2 point and show that some mixed mode chaotic dynamics, reminiscent of spatio-temporal intermittency combining the Turing and the Hopf modes, are also a consequence of the three-dimensional aspect of the structure. The relations between these observations and the theoretical studies performed in genuine two-dimensional systems are still open to discussion.

1. Introduction

A large number of nonlinear systems, maintained far from equilibrium, can produce stationary, boundary symmetry-breaking patterns in spatially extended systems [1]. The chemical patterns predicted by Turing in 1952 [2] have received a renewed interest [3] since their first observation in appropriate open spatial reactors [4]. Turing patterns are quite special; not only they are often proposed as a route to morphogenesis in living things, but contrary to most other pattern forming systems, the wavelength selection does not depend on any geometric dimension of the system (contrary to Rayleigh–Bénard convection cells or Taylor–Couette vortices) and they are not linked to the existence of an interface (at the opposite of capillary waves or Marangoni convection). The critical wavelength of Turing patterns only depends on intrinsic parameters such as rate constants and diffusion coefficients [5, 6]. The corollary is that the Turing instability readily produces patterns that organize in the three directions of space [6], whenever the geometric dimensions of the system make it possible. The originality of Turing structures lies in the conterintuitive organizing role of diffusion, a physical process that usually smears out any concentration gradient. Selforganization originates in appropriate differences in the diffusion coefficients of species involved in the nonlinear kinetic mechanism. Species controlling the positive feedback loop must diffuse slower than any inhibitory species.

For simplicity reasons and mathematical tractability, most theoretical studies were devoted to one- and two-dimensional systems. Also, most hydrodynamic systems can appropriately be accounted for by low dimensionality approaches. Moreover most theoretical and analytical works were performed on systems considered as uniformly constrained in space. In this case, the only spontaneous stable planforms that tesselate the plane are hexagonal arrays of spots and parallel stripes (or bands). In three-dimensional systems, the most stable structures are body centered cubic lattices, columns forming hexagonal prisms, and stacks of parallel sheets [5, 7]. At onset, generally, the first stable patterns in 2D and 3D systems are respectively the hexagons and the bcc structures and the transition from the uniform state is subcritical. Note that in real chemical systems, it is difficult to fulfill the uniform constraint simplifying assumption and, as a result, unexpected planforms are readily observed [8–10].

Moreover, like many nonlinear systems, chemical reaction–diffusion systems can exhibit besides a spatial instability (the Turing bifurcation) a temporal instability (the Hopf bifurcation). A direct transition for stationary patterns to temporal patterns can be obtained as a function of constraints. In the vicinity of this transition, the Turing and Hopf instabilities can couple to produce mixed-mode patterns which often lead to spatio-temporal chaos.

The aim of this paper is to contribute to the understanding of the non standard patterns and complex spatio-temporal patterns experimentally observed in commonly used open spatial reactors. For this purpose we establish and analyse a typical section of the phase diagram of the CIMA reaction. But prior to this, we briefly recall the main features of the reaction and the basic principles of the open spatial reactors used in these and previous experiments.

A Turing instability has been experimentally demonstrated in only one family of liquid phase chemical reactions, the chlorite-iodide-malonic acid (CIMA) oscillatory redox reaction and its variants [11, 12]. The important kinetic steps of the reaction mechanism have been elucidated [13]; iodide (I^-) and chlorite (ClO_2^-) play respectively the roles of the main activator and inhibitor species. The necessary difference in diffusivity between the activator and the inhibitor is obtained by introducing a species of reduced mobility that forms a reversible selective complex with the activator [14–16]. Polyvinylalcohol (PVA), a macromolecule used as an iodine–iodide colour indicator, plays this function in the experiments reported here.

In closed reactors, only transient spatial organizations can be observed [16], precluding appropriate characterization of the stability of states and of the bifurcations

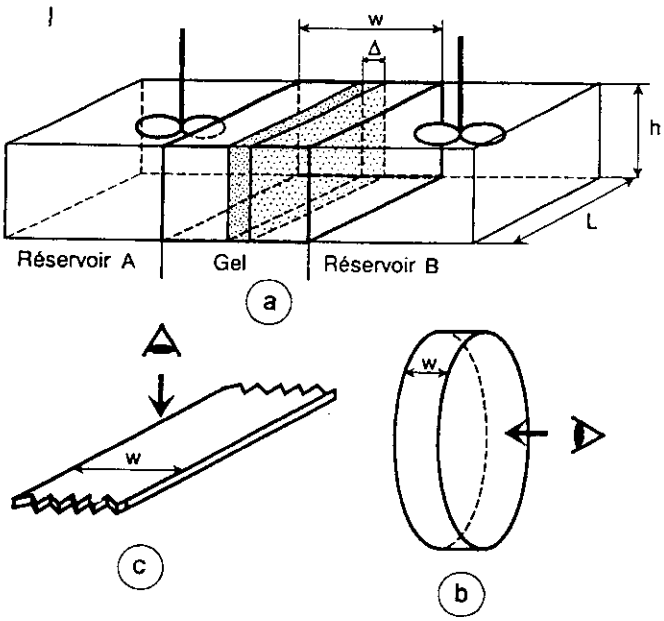

Fig. 1. Sketches of open spatial reactors. (a) Basic principles: The reactor proper consists of a block of hydrogel ($L \times h \times w$) in contact with the contents of two separated reservoirs (A and B). The reservoirs are vigorously stirred and continuously fed with fresh solutions of reagents. L and h are the geometric dimensions of the feed surfaces of the gel reactor and w is the width of the gel, the distance between the reservoirs. Δ is the width over which the chemical pattern, of characteristic wavelength λ, develops. (b) Disc reactor, $L = h \gg w \gg \lambda$. Dimensions presently used: diameter = 21 mm; $w = 3$ mm. (c) Thin strip reactor, $L \gg w \gg h \simeq \lambda$. Dimensions presently used: $L = 20$ mm; $h = 0.2$ mm; $w = 3$ mm.

between them. To overcome this limitation, open reactors were designed to maintain the reaction systems at a controlled distance from equilibrium. The core of these reactors (Fig. 1) is a block of soft hydrogel (polyacrylamide, polyvinylalcohol, or agarose) [5, 6] with two opposite sides in contact with the contents of two stirred tanks filled with two different subsets of reagents. The reagents in the tanks, continuously refreshed by pumps, diffuse into the gel where they react. The other sides of the piece of gel usually correspond to impermeable boundaries. The gel damps out convective fluid motions so that the only processes within the gel are

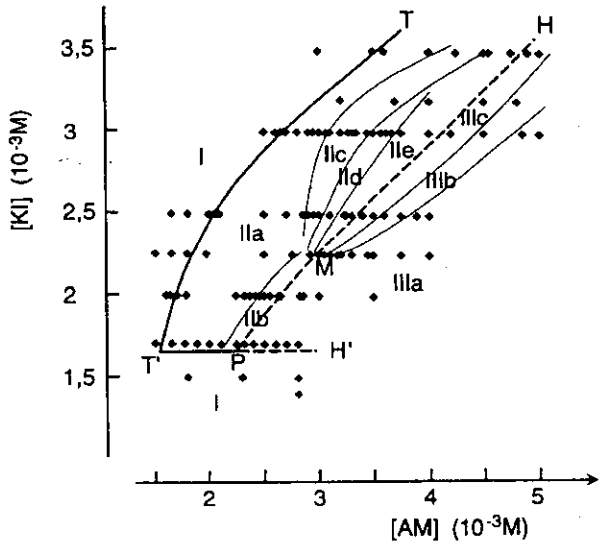

Fig. 2. Pattern phase diagram obtained with the disc reactor. Section in the ($[KI]_B$, $[CH_2(COOH)_2]_B$) plane, all other constraints maintained constant, see text.

reaction and diffusion. With such a boundary control of the system, chemical concentration gradients naturally settle perpendicularly to the feed surfaces, producing isoconcentration planes parallel to these surfaces. Now, one can intuitively understand that in such feed conditions, a spatial or temporal pattern will only develop in a more or less restrained region Δ of the gel, between the feed surfaces. Depending on how the wavelength of the patterns compares with the geometric size of the reactor and with Δ, one-, two- or three-dimensional patterns can develop [5].

Two main geometries of reactors are commonly used: the disc [Fig. 1(b)] and the thin strip [Fig. 1(c)] reactors. They provide complementary views of the patterns in two orthogonal directions. The thin strip allows for a clear determination of the relative width Δ and position of the patterning region between the two feed boundaries. The disc allows for the observation of the pattern organization over the isoconcentration planes. Note also that because of the gradients, different instabilities or pattern modes can be selected at different distances from the feed surfaces. Observations are made with a video camera fitted with macrolens. Images are sent to a frame grabber and contrasts are subsequently enhanced.

2. Experimental observations

2.1. *Experimental conditions*

The experimental conditions are very similar to those used in previous publications of our group [4, 6, 8]. The gel matrix is made of agarose (Fluka Biochemica 05070), 2% weight dry material. It is loaded with Polyvinylalcohol (PVA) (Aldrich, 9000–10 000 MW). PVA is used both as a polyiodide colour indicator and as an agent of reduced mobility complexing the activator. PVA is a better defined and a more easily soluble chemical than strach which was used in our previous experiments. It forms redish–purple complexes in the presence of iodine and iodide species and is colourless in the absence of iodide. However, this colour indicator can slowly diffuse out of the gel; to avoid these losses, PVA was fed into the reservoirs with same concentration as in the gel. Chlorite and iodate in basic solutions were fed onto one side (side A) and iodide and malonic acid in an acetic acid solution were fed onto the other side (side B). Note that in the presence of PVA the solution in reservoir B turns redish–purple because iodine diffuses out of the gel; reservoir A remains clear. During the whole set of experiments, the following constraints were maintained constant: $[KIO_3]_A = 1.88 \times 10^{-3}$ M, $[NaClO_2]_A = 2.0 \times 10^{-3}$ M, $[NaOH]_A = 8.0 \times 10^{-3}$ M, $[CH_3COOH]_B = 2.1$ M, and $[PVA]_{gel} = [PVA]_A = [PVA]_B = 1.5\,g/L$. The residence time τ of the reservoirs is 8.7 minutes, and all experiments were performed at 5 ± 0.1 °C. A phase diagram was established by gradually changing the $[CH_2(COOH)_2]_B$ for different fixed values of $[KI]_B$. The qualitative changes in pattern were tracked down and the transition values determined with more or less refined steps. Each feed composition was maintained for at least 12 h to make sure that the system had reached its asymptotic state; in some cases, close to the different bifurcation lines, the composition was maintained constant over 72 h, because of the slowing down of the pattern settling dynamics. Each feed composition was repeated several times and the reproducibility of the experi-

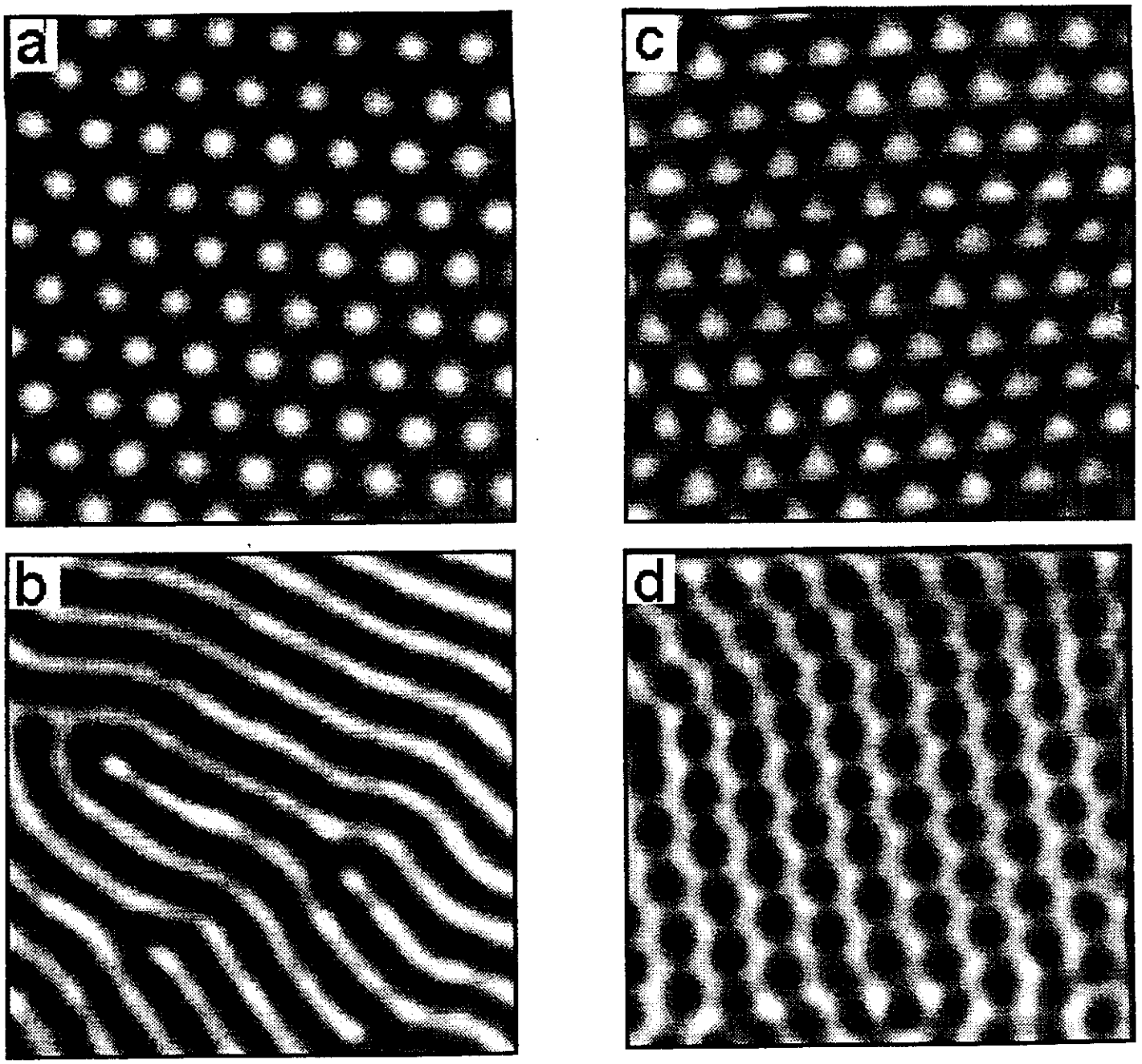

Fig. 3. Stationary planforms observed in the disc reactor. Standard patterns: (a) hexagonal array of "clear" spots from region IIa ($[KI]_B = 2.0 \times 10^{-3}$ M; $[CH_2(COOH)_2]_B = 2.25 \times 10^{-3}$ M); (b) array of parallel stripes (bands) from region IIb ($[KI]_B = 2.0 \times 10^{-3}$ M, $[CH_2(COOH)_2]_B = 2.5 \times 10^{-3}$ M). Nonstandard patterns: (c) array of symmetric triangles from region IIc ($[KI]_B = 3.0 \times 10^{-3}$ M, $[CH_2(COOH)_2]_B = 3.2 \times 10^{-3}$ M); (d) array of "dark" hexabands from region IId ($[KI]_B = 2.5 \times 10^{-3}$ M, $[CH_2(COOH)_2]_B = 3.1 \times 10^{-3}$ M). All patterns are at the same scale: view size 1.7 × 1.7 mm.

ments over different separated runs was better than 10%. The resulting phase diagram was plotted on Fig. 2; it can be divided into three main regions: Region I corresponds to the uniform state (no symmetry breaking pattern) observed at low $[MA]_B$ and at $[KI]_B$ below 1.68×10^{-3} M; region II corresponds to stationary Turing patterns; different planforms can be distinguished in this region; region III gathers different time dependent structures. TT'P and HPH' respectively correspond to the Turing and Hopf bifurcation lines. In spite of refined experiments (step changes of about 2%) occasionally performed in the vicinity of these lines, no hysteresis was unambiguously observed as a function of the malonic feed concentration.

At low iodide concentration, the relative malonic acid concentration range over which the Turing pattern develops gradually decreases. This would agree with the trend predicted by the skeletal model proposed by Lengyel and Epstein [14], if one supposes that, in the patterning stratum, the iodine concentration grossly follows that of iodide fed at the boundary of the gel. However, this gradual decrease is suddenly interrupted at a critical iodide feed concentration. Below this value no symmetry breaking pattern and no time dependent structure is observed. The Turing and Hopf bifurcation lines suddenly curve and collide at the point P. This is a Turing/Hopf codimension-2 point around which the two instabilities develop from the uniform stationary state. This is the first determination of such a point in a chemical reaction–diffusion system. Unfortunately the situation is degenerated, since the Turing and Hopf bifurcation lines practically merge together; moreover, the contrast of stationary patterns and waves sharply decreases along the T'PH' line.

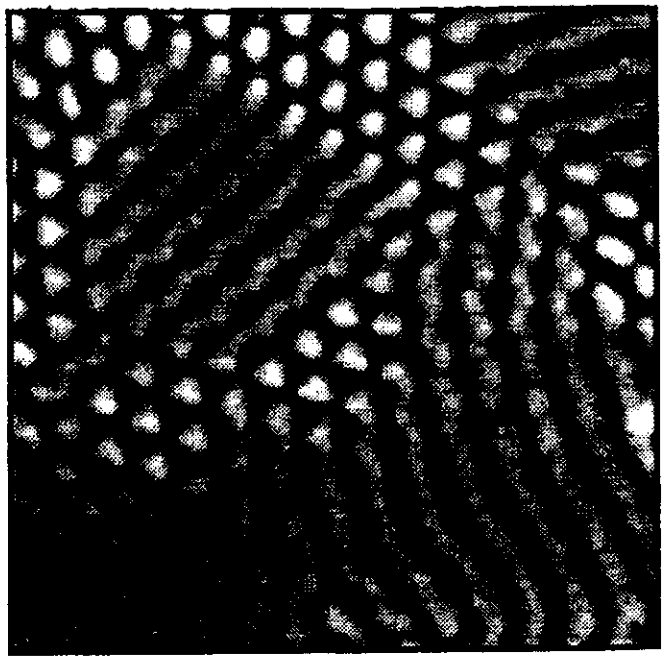

Fig. 4. Mixture of planforms observed in region IIe ($[KI]_B = 3.5 \times 10^{-3}$ M, $[CH_2(COOH)_2]_B = 4.6 \times 10^{-3}$ M); view size 3.0 × 3.0 mm.

2.2. *Stationary patterns*

As predicted by theory of two dimensional systems, the first stable pattern mode observed at onset is an hexagonal array of light intensity maxima (subregion IIa). This region is followed, at low $[KI]_B$ by a domain of stripe (or band) pattern (sub-region IIb). Figures 3(a) and 3(b) illustrate these patterns. Note that close to the point P, the band pattern seems to develop at onset; this would infer that the quadratic term of the Turing normal form drops to zero in this region of the phase diagram [1, 5, 6]. At higher iodide feed concentrations, more unusual templates are observed: They are the symmetric triangles of subregion IIc [Fig. 3(c)], and the mixed hexagon and stripe modes of subregion IId [Fig. 3(d)] – we shall call the latter an "hexa-band" pattern. In addition, an intricate mixture of more or less symmetric triangles, hexa-bands and poorly contrasted stripes is found in subregion IIe (Fig. 4). The transitions between all these new patterns are relatively smooth: patches of coexistent planforms are observed close to the pattern transition regions.

Fig. 5. Wave pattern observed in region IIIa; full view of the disc reactor, average wavelength of the pattern 1.2 mm ($[KI]_B = 2.5 \times 10^{-3}$ M, $[CH_2(COOH)_2]_B = 4.5 \times 10^{-3}$ M).

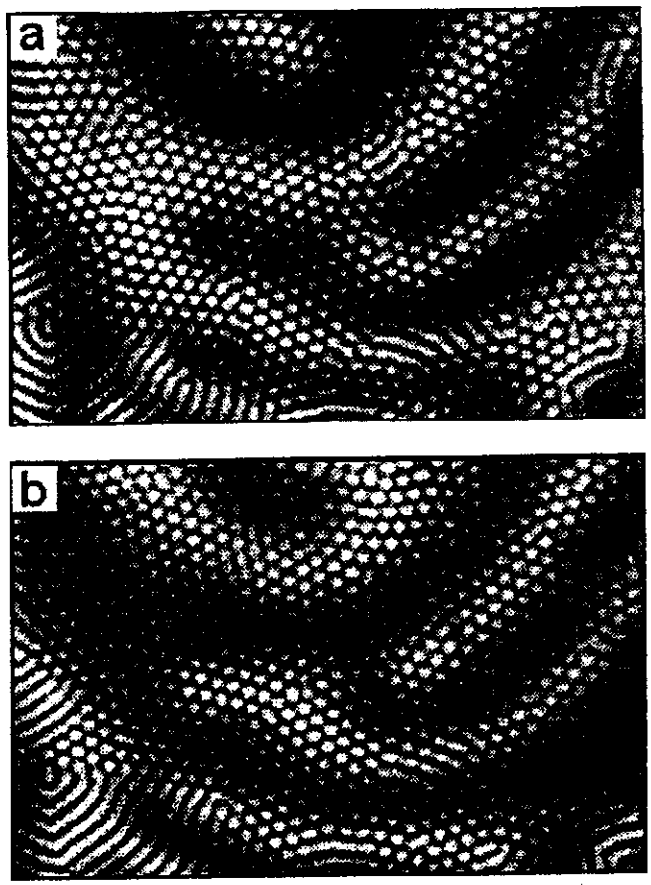

Fig. 6. Superposition of a stationary hexagonal array of "clear" spots and travelling waves from region IIIb. Wave patterns are often more intricate than the one shown here, these were chosen for clarity reasons; (a) and (b) are two snapshots separated by half a period of oscillation. View size 7.5 × 5.0 mm.

2.3. *Spatio-temporal patterns*

At high malonic acid feed concentrations, the chemical system exhibits travelling waves. As illustrated on Fig. 5, the wave patterns are not very regular, the wavelength is rather loosely defined, but the period is quite uniform over the whole surface. The mean wavelength and period generally decrease with increasing malonic acid concentration and the contrast or amplitude decrease with the iodide feed concentration. In particular, the amplitude becomes vanishingly small along the PH' transition line. Waves are very sensitive to small inhomogeneities and usually start at the rim of the disc where the boundary conditions are slightly different due to the holding technique of the piece of gel [18]. Many wavefronts spontaneously break and the separated tips of the waves tend to rotate with the same period than the rest of the wave pattern. Note that this differs from triggered waves in excitable media where spirals always tend to induce a higher frequency than the spontaneous bulk relaxation oscillations [19]. The waves observed in the present experiments are phase waves and the origin of the wave breakage is not clearly determined; it could result from an

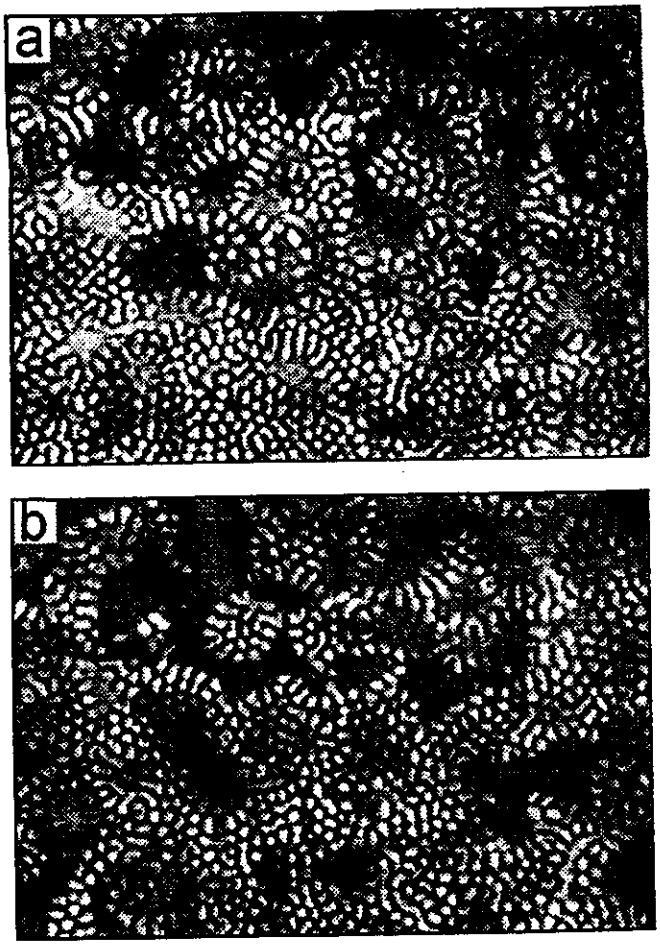

Fig. 7. Turing–Hopf spatio-temporal "turbulence". The two snapshots (a) and (b) are taken at half-an-hour interval and illustrate the complex pattern dynamics observed in region IIIc.

intrinsic instability [20] of the wavetrain dynamics or from small inhomogeneities in the texture of the gel. The latter are difficult to totally eliminate from experiments. Wave breakages are not totally randomly distributed over the surface but they are not always precisely located at one place either. The spiraling tips of the waves tend to drift away from the place they were formed. From time to time, two counterrotating spirals annihilate on head on collision.

The transition from the stationary Turing patterns of region II to the plane wave state of region IIIa can be direct, along the MP portion of the Hopf bifurcation line, or indirect, through a series of complex spatio-temporal behaviours where both waves and Turing like patterns are associated. The direct transition is sharp and, as mentioned above, exhibit no detectable hysteresis.

In the neighbourhood of the MP transition line, depending on the direction of the supercritical change, one or the other state slowly invades the other with a sharp transition front between the two states. The oscillatory dynamics does not penetrate over more than one Turing wavelength into the stationary stripe (band) structure. Furthermore, the transition front acts as a wave source [8].

At high iodide concentration, above point M, two different mixed mode states are observed: In subregion IIIc, the mixed mode appears as a stationary hexagonal pattern over which wavelike changes of the intensity are superimposed (Fig. 6); the two modes seem to very little interact in this region of control parameter. In contrast, waves and Turing like patterns strongly interact in subregion IIIb. This new spatio-temporal structure, is characterized by a less ordered Turing mode superposed by irregular waves and scattered with more or less large "holes" dominated by the sole oscillatory Hopf mode. Figure 7 provides a snapshot of such a spatio-temporal structure. The "Hopf-holes" correspond to the large uniform grey patches surrounded by regions of smaller mosaic-like structures, the Turing mode. The dynamics of the system never settles into a regular spatio-temporal pattern, even after several hours: While the Hopf-holes are slowly invaded by the irregular Turing mode, conversely, new holes suddenly appear inside the Turing mode texture at other random locations. The Turing mode evolves on a time scale slower than that of the oscillations. The waves start at the rim of the holes and the phase of the oscillations tends to organize, from hole to hole, in such a way that a phase difference of π establishes between adjacent oscillatory holes. A more detailed description of the dynamics can be found in Ref. [8].

3. Discussion

It is natural to assume that at onset the width Δ of the pattern stratum is minimum and that it is likely to grow as the system is moved away from the uniform state. Theoretical calculations show [21] that in three-dimensional systems with parameter gradients that mimic our experimental procedure, Turing patterns initially develop in monolayers. At onset, monolayer patterns follow the same pattern selection rules as genuine two-dimensional systems but the bifurcation is delayed until $\Delta \sim \lambda/2$. The first transition is generically subcritical and leads to a fully developed layer of beaded structures with hexagonal symmetry. It is followed by a pattern made of columns laying on the initial iso-concentration planes with an overlap of the stability ranges of the respective structures. By projection on a plane perpendicular to the gradients these beads and columns are viewed as 2D hexagon and band planforms. No other stable planform is predicted for monolayers close to onset. This is just what it is observed in the phase diagram (Fig. 2) at low iodide feed concentration, except that no hysteresis is observed as a function of $[MA]_B$ at the transition lines. The parameter range over which states overlap could be so narrow that the small inhomogeneities of our system would always nucleate a transition to the most stable state.

At a distance from onset, monolayer theory predicts a new generic feature, the restabilization of the hexagonal modes [21]; this type of phenomenon is often referred as re-entrance [22]. Beyond the case of monolayers, there is no systematic theoretical studies of pattern selection in continuous 3-D systems with steep parameter gradients. New types of stable planforms could be expected with $\Delta > \lambda$. In this respect, it is attractive to think that the nonstandard patterns observed in subregions IIb, IIc and IId are generated by "outgrowths" of the monolayer patterns in the third direction to form a more or less separated second layer of patterns. This would be consistent with the fact that the nonstandard planforms are always observed at a distance from the Turing bifurcation lines.

It is a difficult technical task to directly solve the three-dimensional organization of the chemical patterns by optical means, because the patterns are not sharp objects

and the light intensity contrasts decrease with the decrease of focal depth, thus with spatial resolution; also the pattern contrast (amplitude) changes with the local values of the parameters. Nevertheless, experiments performed in thin strip reactors, can provide a direct information on the location and width of the patterning region between the two feed boundaries. Different complementary sets of experiments were performed with such a reactor geometry with the same feed composition, residence time τ of the reservoirs, and temperature T as in experiments performed in the disc reactor. Though experiments performed in so different reactor geometries are not always easily comparable in the details, the gross features of the phase diagram are preserved. The colour profiles viewed in the strip reactor are composed of several parts explained elsewhere [4, 6, 8, 10]; the patterns of interest to us are those breaking the boundary feed symmetry. The experiments in the thin strip reactor show that at low iodide feed concentration either only one row of spots (stationary Turing pattern) or a train of waves with a small extent in the direction of the gradients are observed as a function of malonic acid feed concentration. Figures 8(a) and 8(b) illustrate these features. At high iodide values, two (and even three) rows of spots can be observed at intermediate values of malonic acid concentration [Fig. 9(a)]. On gradually increasing $[MA]_B$, first the most internal row of Turing pattern loses stability and give place to waves. At that time, the wavetrain only "weakly" interacts with the row of stationary spots. This interaction basically produces [Fig. 9(b)] an elongation or even a brief spot splitting in the direction of the gradients as the clear (oxidized) phase of the wave passes by; but spots recover their original shape under the dark (reduced) phase of the wave and their positions remain unchanged. On further increasing $[MA]_B$ [Fig. 9(c)], waves "strongly" interact with the stationary pattern which can then be partly erased from place to place. After some time, the stationary Turing mode grows again at these locations and is erased again a while later. Finally, at still higher $[MA]_B$ the Turing mode completely vanishes and only travelling waves extending over a width Δ larger than the Turing wavelength λ are observed [Fig. 9(d)]. These complementary observations support the idea that the stationary nonstandard planforms and the complex spatio–temporal structures viewed in the disc reactor correspond to two-dimensional projections of actually three-dimensional organizations.

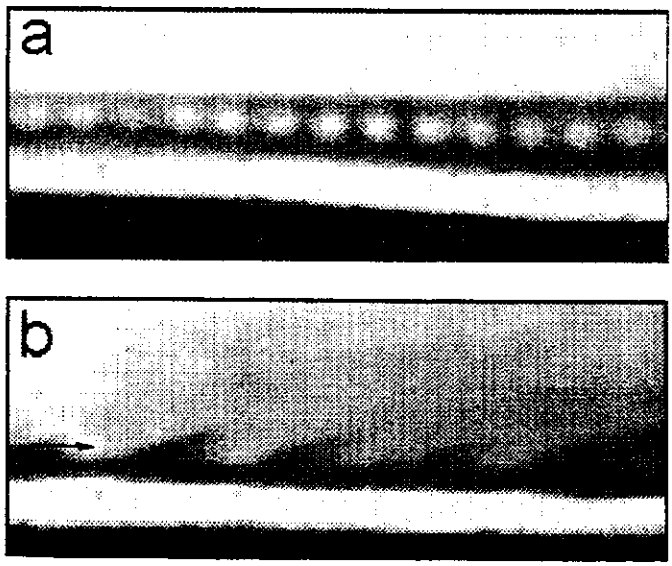

Fig. 8. Patterns observed in the thin strip reactor. At $[KI]_B = 1.5 \times 10^{-3}$ M; (a) single row of stationary spots obtained at low malonic acid feed concentation. (b) wave pattern travelling parallel to the feed boundaries (horizontal) found at higher malonic acid feed concentration; note that the extension of the waves in the direction of the feed gradient is small, of the order of λ. Arrows indicate the direction in which the wave pattern propagates.

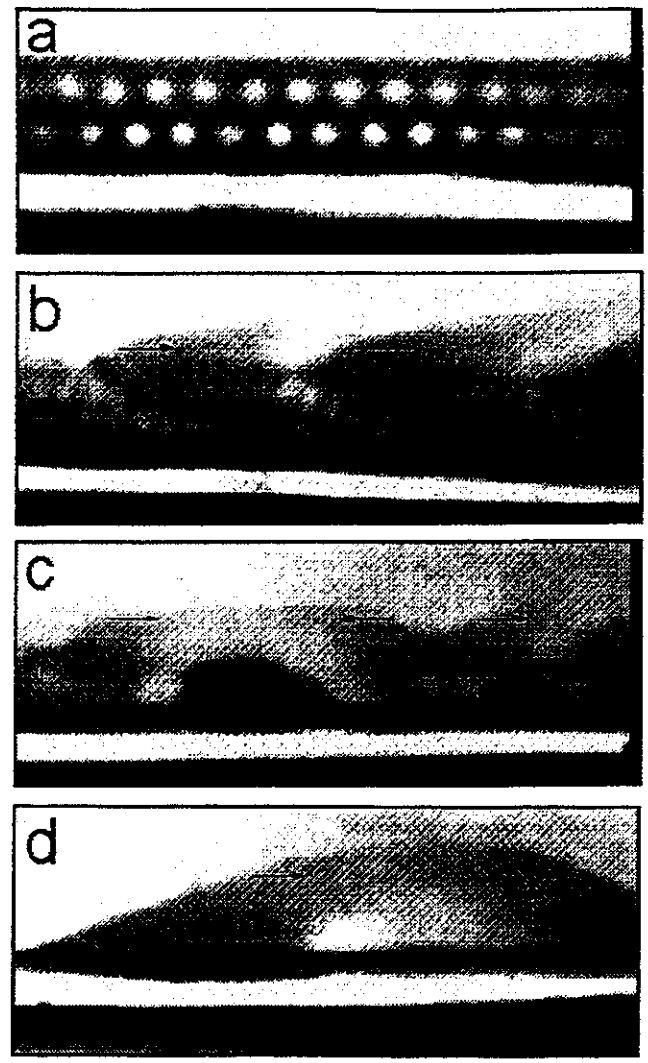

Fig. 9. Patterns observed in the thin strip reactor. At $[KI]_B = 3.0 \times 10^{-3}$ M: (a) Double row of stationary spots; (b) one row of stationary pattern next to travelling wave patterns, arrows indicate the direction of wave propagation; (c) intricate wave and transient stationary spot pattern; (d) travelling wave pattern observed at high malonic acid feed concentration (case of a wave sink), note the large extension of these waves in the direction of the feed gradients. Arrows indicate the direction of the travelling wave patterns. All snapshots are taken at the same scale: view size 2.6 × 1.0 mm.

Numerical calculations show [23] that in the presence of parameter gradients, patterns with different symmetries can develop at different locations along these gradients. Previous experimental observations [6, 8, 24] are consistent with the above mentioned numerical results. The main open question concerns the possible stable phase relations between the different adjacent planforms. The triangular patterns of subregion IIc can be produced by a moiré effect due to the superposition of a layer with an hexagonal array of clear spots and a layer with an hexagonal array of dark

spots with the spots of one array on the top of every two lacuna of the other. Though only stable monolayer arrays of clear spots have been obtained, monolayers of black hexagons have been observed as transients, in these and other experimental conditions [6, 10, 24]. The dark hexa-band patterns, in subregion IId, can correspond either to the superposition of a layer of columns and a layer with an hexagonal array of dark beads with the lines of beads in phase with the dark phase of the columns, or to the superposition of two layers with hexagonal arrays of clear beads slightly off their respective lacunarity positions. The first hypothesis would be more in the continuity of the interpretation for the triangles but the second cannot be totally rejected at the present time.

Recently Bestehorn [25] has performed a stability analysis of the global patterns resulting from the linear coupling of two normal form equations for Turing in two planes which differ by the value of their quadratic terms – a parameter which controls the sign and stability of the hexagon patterns [1, 5, 6]. He shows that in these conditions, symmetric triangles and the hexa-band mixed modes are stable global patterns which respectively result from the coupling of hexagons of reverse signs and of hexagons and bands. However, the bifurcation sequence predicted by these calculations does not agree with the experimental observations. In the calculations the standard hexagonal planform is separated from the triangular planform either by hexa-bands or by stripes; in experiments the triangles (subregion IIc) follow immediately the hexagons (subregion IIa). The difference might come from the discrete nature of the two plane model which contrasts with the spatial continuum in the third direction of the real system. The sequence and the possible stable phase relations between the different layers of patterns could also depend on the shape of the confining parameter well. Also the neighbouring uniform modes should be taken into account since they can enhance quite dramatically the stability of the hexagonal modes [22].

The spatio–temporal behaviours reported here have already been described in a previous publication [8]. It was suggested that the class of spatio–temporal structures found in subregion IIIc results from the simple superposition of a space instability and a time instability living in two adjacent layers, but the effective dimensionality of the spatio–temporal intermittency found in subregion IIIb was until now unclear. Theoretical calculations show that the coupling between the Turing and the Hopf instabilities can lead to a mixed mode and to spatio–temporal chaos in one- and two-dimensional systems [27]; the latter chaos is reminiscent of observations made in subregion IIIb. Now, the present experiments show that the phase diagram domains corresponding to dynamical behaviours suggestive of a Turing–Hopf interaction disappear below the same critical iodide feed value than the nonstandard stationary patterns which we have attributed to pattern outgrowths in the third direction. This leads us to think that the observed Turing–Hopf intermittency heavily relies on the structure organization in the third direction. The spatio–temporal dynamics observed in subregion IIIc and IIIb are probably both the result of the spatial coupling of a Turing and a Hopf instability turned on in adjacent planes. This assumption is further supported by the observations performed in the thin strip reactor. Though spatio–temporal intermittency can be obtained in genuine 2-D systems, it seems that the three-dimensional aspects play an important role in experiments. When the spatio-temporal pattern confinement width Δ is reduced to the size of λ, the Turing–Hopf mixed mode and intermittent dynamics disappear. Only the plane wave patterns remain. However, the spiral defects of these waves exhibit a quite interesting peculiarity: A finite amplitude corresponding to an elementary Turing cell forms the core of the spirals [8]. Note that, the amplitude of this residual Turing mode decreases as the system is driven away from the HP bifurcation line. It is also worth mentioning that the present observations do not preclude that quasi-2D Turing–Hopf modes might exist for other experimental conditions.

4. Conclusion

Though it is difficult to make a direct analysis of the three-dimensional organization of chemical patterns, we argue that the stable triangular and hexa-band mixed mode patterns, observed in an extended disc reactor, originate in the interaction of different classical hexagon and band planforms developing at adjacent positions between the feed boundaries. Triangles and hexa-bands can be obtained by moiré effects from the superposition of an hexagonal array of dark spots with respectively an hexagonal array of clear spots or an array of stripes. Using a new type of disc reactor which allows for the unfolding in space of a sequence of pattern transitions, we have recently observed [10] stable moiré patterns resulting from the overlay of an array of clear spots and an array of stripes with the lines of spots in concordance either with the clear phase or with the dark phase of the stripes. Furthermore, staggered layers of bands were identified in these experiments. Other nonstandard pattern planforms were also reported by another group; in particular, an array of clear spots exhibiting an harmonic substructure, dubbed "black eyes", is reported [9]. The unharmonic features of these seemingly 2-D patterns could be excited by the longitudinal instability, that is the instability growing in the direction of the parameter gradients.

Summarizing, the presence of steep parameter gradients in one direction of an extended three-dimensional system makes pattern selection mechanisms more versatile than genuine two- or three-dimensional systems with uniform constraints. Though there are a few promising theoretical results on pattern selection in systems in the presence of parameter gradients, further advanced analysis are still necessary in order to determine which are the relevant features that control the stable phase relations between the successive "layers" of pattern modes and if the parameter gradients can play a role in the excitation of unharmonic terms.

In the case of the observed spatio–temporal structures, it is still unclear if the dynamics obtained by coupling regions of space with different autonomous space and time instabilities can be readily compared with the Turing–Hopf mixed modes computed for genuine 2D systems. In this respect more theoretical work should be performed around the Turing–Hopf codimension-2 point in systems submitted to steep gradients of constraints.

The understanding of pattern selection under nonuniform parameter conditions is of great interest since most natural

systems are not uniformly constrained over space. In particular, these studies could be relevant to biological systems since all biochemical informations and nutrients that come across tissues or cellular membranes can seldom be considered as uniformly spread over space.

Acknowledgements

We thank J. Boissonade, P. Borckmans and G. Dewel for fruitful discussions and R. Deleule for technical assistance.

References

1. Cross, M. C. and Hohenberg, P. C., Rev. Mod. Phys. **65**, 851 (1993).
2. Turing, A. M., Phil. Trans. Roy. Soc. London **B327**, 37 (1952).
3. "Chemical Waves and Patterns" (Edited by R. Kapral and K. Showalter), "Understanding Chemical Reactivity", **10**, (Kluwer Academic Publisher 1994).
4. Castets, V., Dulos, E., Boissonade, J. and De Kepper, P., Phys. Rev. Lett. **64**, 2953 (1990). De Kepper, P., Castets, V., Dulos, E. and Boissonade, J., Physica **D49**, 161 (1991).
5. Borckmans, P., Dewel, G., De Wit, A. and Walgraef, D., Ch. 10 in reference [3].
6. Boissonade, J., Dulos, E. and De Kepper, P., Ch. 7 in reference [3].
7. Walgraef, D., Dewel, G. and Borckmans, P., Adv. Chem. Phys. **49**, 311 (1982). De Wit, A., Bockmans, P., Dewel, G. and Walgraef, D., Physica **D61**, 289 (1992).
8. De Kepper, P., Perraud, J.-J., Rudovics, B. and Dulos, E., Int. J. Bif. Chaos **4**, 1215 (1994).
9. Ouyang, Q., Gunaratne, G. H. and Swinney, H. L., Chaos **3**, 707 (1993).
10. Dulos, E., Davies, P., Rudovics, B. and De Kepper, P., Physica D (to appear).
11. De Kepper, P., Epstein, I. R., Kustin, K. and Orbán, M., J. Phys. Chem. **86**, 170 (1982).
12. De Kepper, P., Boissonade, J. and Epstein, I. R., J. Phys. Chem. **94**, 6525 (1990).
13. Lengyel, I., Rabai, G. and Epstein, I. R., J. Am. Chem. Soc. **112**, 9104 (1990).
14. Lengyel, I. and Epstein, I. R., Science **251**, 650 (1990). Lengyel, I. and Epstein, I. R., Proc. Nat. Sci. USA **89**, 3977 (1992).
15. Pearson, J. E. and Bruno, W. J., Chaos **2**, 513 (1992).
16. Lengyel, I. and Epstein, I. R., Ch. 9 in Ref. [3].
17. Ouyang, Q. and Swinney, H. L., Ch. 8 in Ref. [3].
18. Rudovics, B., PhD Thesis, Bordeaux, France, (October 1995).
19. Zykov, V. S., "Simulation of Wave Processes in Excitable Media" in Nonlinear Science Theory and Application, (Manchester University Press, 1987).
20. Kuramoto, Y., "Chemical Oscillations, Waves and Turbulence", Springer Series in Synergetics, **19** (Springer–Verlag, Berlin, 1984).
21. Dufiet, V. and Boissonade, J., Phys. Rev. E, **53**, 4883 (1996).
22. Verdasca, J., De Wit, A., Dewel, G. and Borckmans, P., Phys. Lett. **A179**, 91 (1993). Dewel, G., Borckmans, P. *et al.*, this issue.
23. Borckmans, P., Dewel, G. and De Wit, A., Physica **A188**, 137 (1992).
24. Ouyang, Q., Noszticzius, Z. and Swinney, H. L., J. Chem. Phys. **96**, 6773 (1992).
25. Ouyang, Q. and Swinney, H. L., Chaos **1**, 411 (1991).
26. Bestehorn, M., Phys. Rev. E, **53**, 4842 (1996).
27. De Wit, A., PhD Thesis, Brussels (September 1993).

Reprinted from

PHYSICA D

Physica D 98 (1996) 53–66

From quasi-2D to 3D Turing patterns in ramped systems

E. Dulos *, P. Davies, B. Rudovics, P. De Kepper

Centre de Recherche Paul Pascal, CNRS, Université Bordeaux I, Avenue Schweitzer, 33600 Pessac, France

Received 18 December 1995; revised 8 March 1996; accepted 8 March 1996
Communicated by F.H. Busse

N·H
ELSEVIER

ELSEVIER

Physica D 98 (1996) 53–66

PHYSICA D

From quasi-2D to 3D Turing patterns in ramped systems

E. Dulos *, P. Davies, B. Rudovics, P. De Kepper

Centre de Recherche Paul Pascal, CNRS, Université Bordeaux I, Avenue Schweitzer, 33600 Pessac, France

Received 18 December 1995; revised 8 March 1996; accepted 8 March 1996
Communicated by F.H. Busse

Abstract

We elaborate on the transition from quasi-two-dimensional to three-dimensional Turing patterns in a chemical reaction–diffusion system confined in gradients of chemicals between two feed boundaries. This transition is observed in open spatial reactors specially designed to make possible the unfolding of a pattern sequence in one direction of the plane of observation. In this direction, the confinement of the structure is progressively relaxed. Complementary observations from two reactor geometries allow the dimensionality of the structure to be elucidated: quasi-two-dimensional and three-dimensional patterns, respectively, correspond to patterns developing in monolayers and in bilayers. Beyond the now classical hexagonal and stripe patterns, various new stable planforms are shown to result from the coupling of these two classical pattern modes which develop in two adjacent layers, with well-defined phase relations between the two pattern modes.

PACS: 05.70.Ln, 47.54.+r; 82.20.Mj; 80.
Keywords: Turing patterns; Reaction–diffusion; Pattern dimensionality; Confined systems; CIMA reaction

1. Introduction

Turing patterns belong to the class of self-organization phenomena that result from a spontaneous symmetry breaking instability in non-linear dynamical systems maintained at a controlled distance from thermodynamic equilibrium. These are stationary concentration patterns of solvated species that result from the sole interplay of molecular diffusion and chemical reaction. Such chemical reactions must involve antagonistic activatory and inhibitory kinetic processes. Turing patterns call for differences in the diffusion coefficients of species, in particular, a species controlling the inhibitory process must diffuse faster than species in control of the activatory process. The patterns are characterized by an intrinsic wavelength, that is wavelength is independent of any geometric dimension of the system. Due to seemingly contradictory requirements for their formation, the first unambiguous experimental observation of Turing patterns [1] occurred nearly 40 years after their theoretical prediction by Turing in 1952 [2]. Besides their fundamental interest in physics [3], their possible implication in certain stages of morphogenesis made them popular among a community of biologists and biomathematicians [4–6].

Most of the theoretical works on pattern formation assume, for mathematical simplicity, that the system be uniformly constrained over space. Under these conditions, it has been analytically determined and confirmed by numerical simulations that only a small number of planforms can spontaneously develop. In

* Corresponding author.

PII S0167-2789(96)00072-3

two-dimensional systems, these planforms consist of hexagonal arrays of dots and parallel stripe patterns [7–9]. In three-dimensional systems, lamella, hexagonal prisms and body centered cubic arrays [10] are such selected patterns.

It is worth noting that in real chemical systems, it is impossible to fulfil the uniform constraint conditions. As we shall see in more detail further on, the experimentally observed Turing patterns develop in systems that naturally involve parameter gradients. These gradients confine the pattern in a more or less narrow region of space where appropriate chemical conditions are met for the Turing instability to develop.

Nonetheless, the effect of parameter gradients in a chemical one-dimensional system was considered form a theoretical point of view during 1970's [11]. It was also theoretically examined in two- or three-dimensional systems, in the framework of patterning models for biological systems [12,13]. In this context, Boissonade [14] provided in 1988 a numerical analysis of a Turing bifurcation in a two-dimensional rectangular system fed only by diffusion from two opposite boundaries, a configuration which naturally leads to gradients of feeding species. These calculations show that at onset, the Turing instability develops a dot pattern orthogonally to the parameter gradients. Our initial experimental observation of sustained Turing patterns followed this more practical approach [1].

Using the CIMA reaction, we have observed patterns developing in successive rows of spots [1,15,16], in perfect agreement with Boissonade's theoretical results [14,16]. Soon after, with the same reaction and a reactor more extended in the third direction, Ouyang and Swinney produced spot and stripe patterns [17,18] analogue to those predicted in extended two-dimensional systems; these patterns tessellate planes that extend in the third direction of the reactor. Some of our experiments indicated that pattern can be three-dimensional [19]. Ouyang et al. rather produced apparently two-dimensional patterns [17,18,20]; then, they also considered the development of three-dimensional patterns. Further experimental observations show that different patterns can develop at different distances to the feed boundaries [21] and that the dimensionality of patterns may depend on some geometric size of the reactor [22]. More recently, we have published a preliminary observation of three-dimensional patterns consisting either of two contiguous planes tessellated with stationary patterns or of one plane of stationary patterns and one with travelling waves [23,24].

Here, we report on experiments performed in reactors designed to elucidate how two-dimensional patterns evolve to three-dimensional patterns as the confinement in the third direction is gradually relaxed. We also examine the transition between different types of two-dimensional patterns under a slow parameter ramp. We emphasize that there are no genuine two-dimensional experimental patterns but rather patterns developing in monolayers and we discuss the experimental patterns in monolayers in connection with actually two-dimensional patterns produced by simulations. The experimental conditions (reactors and reaction) used for the reported experiments are indicated in Section 2. We describe in Section 3 the patterns observed first in the asymptotic state of the system, then in a transient situation. Finally these experimental results are discussed in Section 4, in the light of results of theoretical studies and simulations of such systems, and taking into account the dimensionality of the patterns.

2. Experimental conditions

2.1. Reactor

The core of the reactor is a piece of soft hydrogel with two opposite faces in contact with solutions of reagents kept in two reservoirs I and II (see Fig. 1(a)). Starting from these faces, reagents diffuse into the gel where they meet and react. The other sides of the piece of gel correspond to impermeable boundaries. The gel prevents the chemical reacting medium from any convective fluid motion so that the only active processes inside the gel are the reaction and the molecular diffusion of species. Solutions in reservoirs I and II are permanently renewed by pumps and continuously stirred, ensuring constant and uniform boundary conditions. Reagents are distributed in

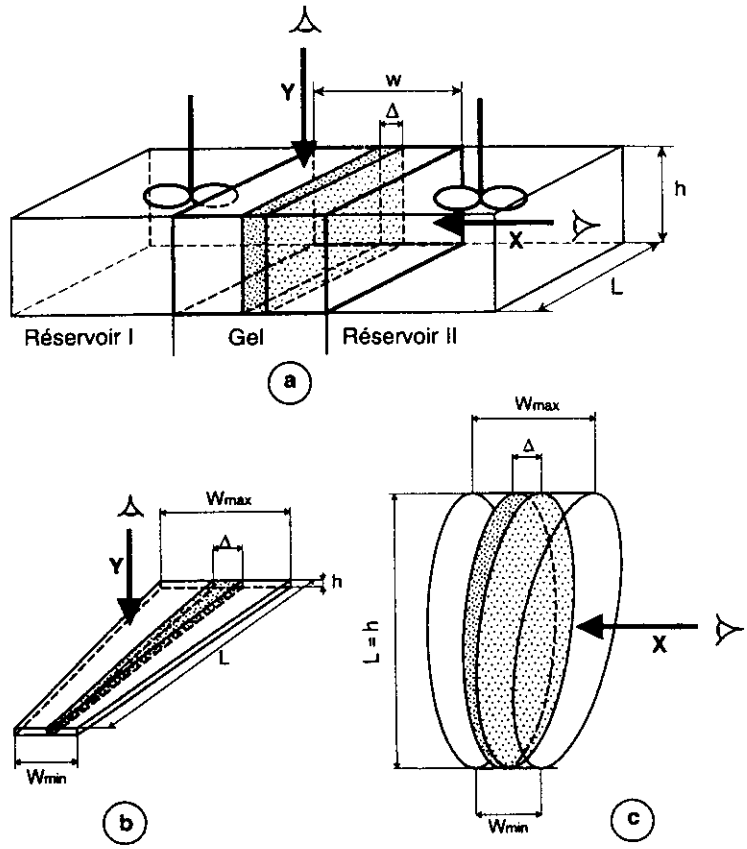

Fig. 1. Sketches of the open spatial reactors. (a) The basic principle: the piece of gel ($L \times h \times w$) is in contact with the contents of stirred reservoirs I and II; Δ is the width of the pattern-forming region. Observations are made from above (arrow y) in the thin strip reactor (with dimensions $h \leq w < L$), and perpendicularly to the feed surfaces in the disc reactor (diameter $L = h$). (b) and (c) The bevelled thin strip and disc reactors. In the thin strip $h = 0.2$ mm; in both reactors: $W_{max} = 3.5$ mm, $W_{min} = 1.75$ mm, $L = 25$ mm; Arrows y and x indicate the observation directions.

reservoirs I and II in such a way that neither of the solutions is separately reactive and, due to the differences in their compositions, strong concentration gradients of chemicals naturally settle in the gel perpendicularly to the feed surfaces, leading to iso-concentration planes parallel to these surfaces. Generally, the appropriate conditions for the development of a reaction–diffusion instability are only met in a restricted region of width Δ between the two feed surfaces: Δ depends on such parameters as the concentrations of feed species and, of course, on the distance w between the feed surfaces. Depending on how the wavelength λ of the pattern compares with the dimensions Δ, L and h of the pattern-forming region (Fig. 1(a)), one-, two- or three-dimensional spatial patterns can develop.

Two different geometries of reactors – the thin strip reactor and the disc reactor – have been derived from the general scheme in Fig. 1(a) as follows.

2.1.1. Thin strip reactor

The thin strip reactor is made of a thin narrow rectangular piece of gel ($L \gg w > h$; typically $h < 1$ mm). The gel strip is fed by the two long edges ($L \times h$). Observations made as above (see arrow y in Fig. 1(a)) provide a direct view of the area that extends between the feed surfaces. In particular, the location and the width Δ of the pattern-forming region

can immediately be seen. Pattern develops in rows of spots or in stripes parallel to the feed boundaries, that is orthogonal to the initial ramps of chemicals. The initial observations of Turing patterns were performed in a thin strip reactor [1,15,16]. If the gel strip is thin enough (h of the order of the wavelength λ of the structure), it approximates a two-dimensional rectangular system. Then one-dimensional or two-dimensional patterns can be obtained, depending on whether they develop on one or more rows.

2.1.2. Disc reactor

The disc reactor is made of a flat disc of gel with a thickness w. In this geometry, the faces $L \times h$ in Fig. 1(a) are circles with a diameter $L = h$. The disc is fed by these two circular faces. Observations made perpendicularly to the feed surfaces (arrow x in Fig. 1(a)) give a view of planes parallel to these faces, that is in a direction perpendicular to that used in the thin strip reactor. The disc reactor was first used by Ouyang and Swinney [17,18]. With this geometry of reactor, patterns made of arrays of spots or of stripes readily spread over the whole plane of observation. An obvious advantage of this reactor geometry is to allow for observation of patterns extended over large planar areas of uniform parameter values; but it obscures the pattern development in the third direction (that of the ramps of chemicals).

Summarizing, pattern in the thin strip reactor usually appears as rows of spots while it extends over planes in the disc reactor. Further these rows and planes are parallel to the feed boundaries in both reactor geometries.

2.1.3. Bevelled gel reactors

The reactors in Section 2.1 were slightly modified for the experiments reported here. The feed surfaces are no longer parallel but make an angle. Both bevelled thin strip and disc reactors (Figs. 1(b) and (c)) were used. In such geometries, w, the distance between the feed surfaces changes continuously from 1.75 to 3.5 mm over a length (or diameter) L of 25 mm. Thus, the feed surfaces make an angle of 4°.

The slant between the feed surfaces introduces a slow continuous change in control parameters along the plane of observation. Indeed, the gradient in w produces a gradual change in the concentration ramps across the gel, which results in a gradual change in Δ, the width of the patternforming region. As a consequence, the number of rows (or planes) of patterns gradually changes from one end to the other of the bevelled piece of gel. In addition, since the chemical processes within the gel are non-linear, the chemical composition along one row (or plane) will also gradually change. In such conditions, we can expect different types of patterns to develop in the direction of the slope.

Images were acquired with a black and white video CCD camera fitted with macrolens and attached to a personal computer. Subsequently, a picture processor was used to enhance the grey level contrasts.

2.2. Gel

Experiments were performed in a polyacrylamide gel loaded with thiodène [1]. Thiodène is an iodine colour indicator from Prolabo, containing 7% soluble starch [25], the excipient is washed out of the gel prior to use. The pieces of gel were made with a solution of the following composition per 100 ml: 2 g of acrylamide, 0.46 g of N, N'-methylenebisacrylamide, both from Aldrich and 3 g of thiodène. Polymerization occurs in about 10 mm at 0°C.

2.3. Reaction

Experiments were conducted with the chlorite–iodine–malonic acid oscillating reaction [26] currently referred as the "CIMA" reaction. Based on a skeleton kinetic mechanism of the reaction, it was proposed [27] that iodide (I^-) and chlorite (ClO_2^-) play, respectively, the roles of the activator and of the inhibitor species. It was also proposed [27–29] that starch, a macromolecule immobilized in the gel network (or any immobilie functional site of the gel), that makes a reservible complex with the activator, plays a key role in the formation of Turing patterns. This assumption was experimentally corroborated [30].

The reagents were distributed as follows in the reservoirs: Iodide and malonic acid in sulphuric acid solution were fed on one side. Iodate and chlorite in basic solution were fed on the other side. Note that on the chlorite side, the reservoir was fed with iodate instead of iodide. Indeed, when fed on this side, iodide is rapidly oxidized to iodate near the corresponding feed surface of the gel.

Since the oxidizers, chlorite and iodate, are only on one side, the oxidation capacity of the chemical medium inside the gel decreases from that side to the other. Consequently, near the chlorite side, the iodine species are oxidized and the gel remains colourless. Near the malonic acid side, iodine species are present mostly under their reduced forms I^- and I_2 which produce a dark blue complex with starch enclosed in the gel. Thus, along this side, the gel becomes dark.

The residence time was identical in both reservoirs and had the same value for both types of reactors. All feed parameters and bath temperature (4°C) were identical in reactors of both types in order to enable us to compare observations.

3. Experimental results

3.1. Global description

Figs. 2 and 3 give an example of the unfolding of patterns observed in our two types of bevelled reactors for a same set of feed concentrations. The figures provide a global view of the bevelled gel strip and disc after 36 h.

As already mentioned, the directions of observations for the two reactor geometries are orthogonal. The symmetry breaking pattern in the thin strip reactor appears as rows of spots parallel to the feed edges of the strip. In the disc reactor, a much wider variety of patterns tesselating the plane is observed.

Due to the small wavelength of the patterns (about 0.13 mm) and the pixel resolution of the CCD camera, macrolens were used to obtain pictures of patterns with enough resolution. Consequently, only a small part of the reactor is viewed at one time; the images of the whole bevelled pieces of gel can be reconstructed by placing side by side several pictures such as those presented in Figs. 2 and 3. Note that the magnification of Fig. 2 is greater than that of Fig. 3. In all the cases, larger magnifications of selected areas are provided when necessary. Note also that the focal depth of the optical set-up used in the reported experiments is of the order of 1 mm.

3.1.1. In bevelled thin strip

The experiment presented in Fig. 2 was performed with a gel strip 0.2 mm thick. The width of the strip increases from Fig. 2(a) to Fig. 2(e) and from left to right in each figure. The figures only show the side of the strip that bears patterns. Each figure exhibits from bottom to top: (i) a first dark band that develops next to the malonic acid fed boundary located along the bottom of the pictures, followed by (ii) a clear band parallel to the preceding dark one, and (iii) a second dark band parallel to the other bands, inside which a pattern of clear dots develops; the width of this band increases with the width of the strip; beyond this, (iv) a clear zone extends over the rest of the strip.

Let us now focus on the second dark band. Typically, as the width of the gel strip increases, a spot pattern emerges in that region; the spots organize in one, then two rows parallel to the feed boundaries:

- In the narrowest part of the strip (Fig. 2(a)), no spot pattern is observed: in this region of the gel, no symmetry breaking pattern develops.
- In the following part (Fig. 2(b)), the clear spot pattern breaking the boundary symmetry emerges and develops over one row. Note that the pattern becomes fuzzy at the right end of this figure.
- In the widest parts of the strip (Fig. 2(d) and (e)), the width of the region of symmetry breaking pattern has increased and the pattern is essentially made of two rows of spots. However, at some locations, the amplitude of the spot modulation decreases or even disappears (right end of Fig. 2(d), left end of Fig. 2(e)), giving place to a more or less uniform clear band. At the very end of the gel strip (right end of Fig. 2(e)), the two rows can fuse back into one. Indeed, the parts holding up the gel at each end may introduce defects of feed in the first and last

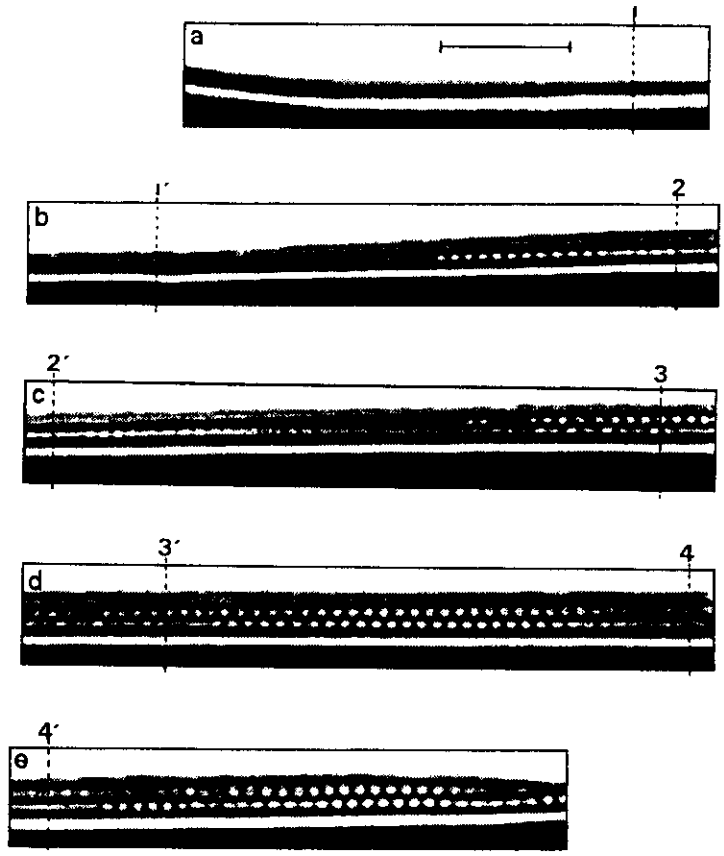

Fig. 2. Patterns in the bevelled thin strip. (a)–(e) are the binarized images of five successive portions of the strip. The whole pattern sequence can be reconstructed by placing side by side the five successive images. Pairs of vertical dotted lines (1 and 1′, 2 and 2′, etc.) indicate the same location along the strip. The bar inside (a) corresponds to 1 mm. (a) no symmetry breading pattern; (b) no symmetry breaking pattern and symmetry breaking pattern forming one row of spots; (c) transition region between one and two rows; (d) and (e) symmetry breaking pattern forming two rows of spots. Experimental conditions: concentrations of reagents in reservoir I: $[NaClO_2] = 0.0475\,M$, $[NaOH] = 1.2 \times 10^{-2}\,M$, $[KIO_3] = 2 \times 10^{-3}\,M$; in reservoir II: $[AM] = 1.3 \times 10^{-2}\,M$, $[H_2SO_4] = 10^{-2}\,M$; $[KI] = 2 \times 10^{-3}\,M$, $[Na_2SO_4] = 3 \times 10^{-3}\,M$; temperature = 4°C; residence time of reservoirs = 6 min.

5% along the length of the strip (see also the left end of Fig. 2(a)).

- The transition between one and two rows can be seen in Fig. 2(c). A magnification of such a transition region is given in Fig. 4. At the approach of the transition region, the modulation of the light intensity in the single row rapidly decreases: spots almost disappear. Then, as this fuzzy region becomes wider, a new clear spot pattern gains consistency. These spots elongate before separating in two spots of unequal sizes. The resulting pairs of spots first arrange obliquely in the pattern band. Then, as spots in the pairs become more equal in size and intensity, the pairs tilt in the direction of the feed gradient, giving rise to the appearance of a second row of spots. Progressively, a shift appears which then increases between the two spots of each pair. The final arrangement in two rows of perfectly staggered spots is reached at the right end of Fig. 4(b) (and in the middle part of Fig. 2(c)).

Thus, the emergence of the second row of spots as the width of the pattern region increases, is very progressive. It proceeds through some sort of spot division followed by the separation of the second

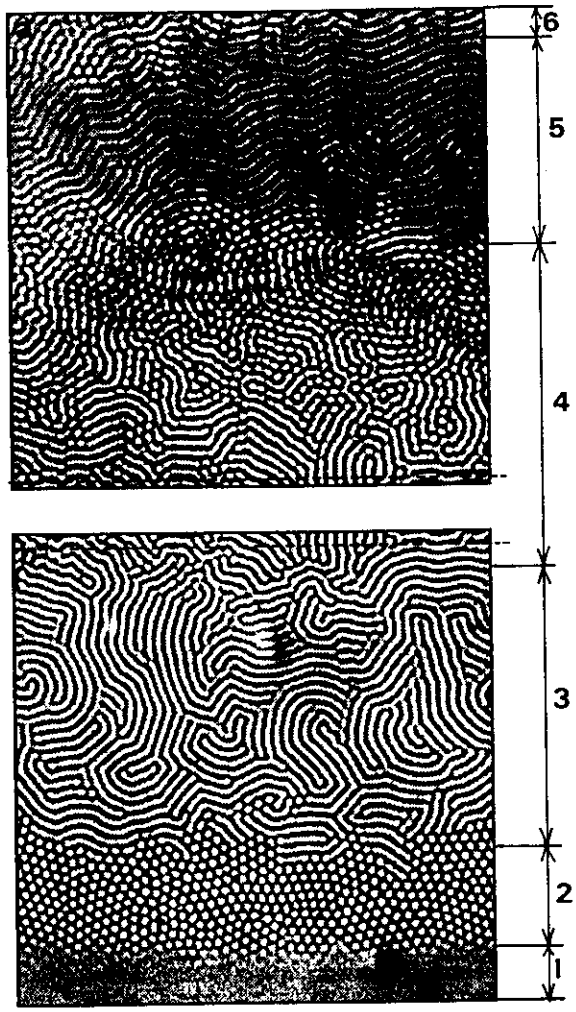

Fig. 3. Sequence of pattern in the bevelled disc. The whole sequence can be reconstructed by juxtaposing (a) and (b) and superposing the dotted lines at the top of (a) and at the bottom of (b). The various patterns extend over parallel bands. The vertical arrows delimit their successive domains: 1. uniform state (truncated at the bottom of the figure); 2. hexagonal array of spots; 3. stripes; 4. mixture of stripes and spots; 5. asymmetric stripes; 6. "non-standard" planforms. Experimental conditions as in Fig. 2(a) and (b): view size 6.9 mm × 6.9 mm.

row from the first one and by a progressive increase of the phase shift between spots in the two rows.

3.1.2. *In bevelled disc*

Each picture in Fig. 3 gives a view of about half the height of the disc in the median region; the lateral parts not shown bear the same types of patterns. The

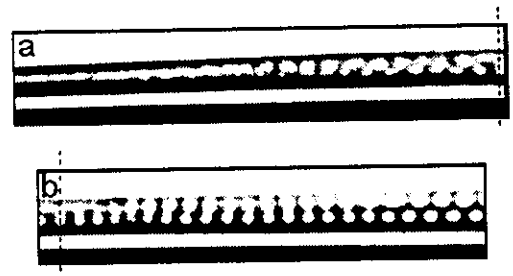

Fig. 4. The transition region between domains with one and two rows of spots, in the bevelled strip. The whole sequence can be reconstructed by placing side by side images (a) and (b). The vertical dotted lines indicate the same location along the strip. Form left to right in each figure: (a) fuzzy pattern with a few clear spots, spots of large size, spots splitting in two spots obliquely arranged; (b) pairs of spots arranged more or less perpendicularly to the feed boundary, two rows of staggered spots.

thickness of the disc progressively increases from the bottom of Fig. 3(b) to the top of Fig. 3(a). Patterns of different types extend over successive regions (numbered on the figure). These regions are almost parallel and organize as follows with the increasing thickness of the disc:

1 – a narrow uniform (structureless) region;
2 – a region of clear spots exhibiting a hexagonal arrangement;
3 – a wide domain of stripes;
4 – a region of complex organization exhibiting an intricate mixture of spots and stripes;
5 – a region of less contrasted, asymmetric stripes;
6 – a region of very intricate planform, located at the top of the disc.

The global organization can hold for days without significant modification of the general pattern. The area covered with patterns as well as the relative extent of the domain of each type of planform depend on the feed concentrations. The pictures of Fig. 3 were obtained with a chlorite concentration ($[NaClO_2]$) of 0.0475 M in the reservoir. In this case, the structureless region 1 extended over one eighth of the height of the disc. When $[NaClO_2]$ was increased by 30%, the extent of region 1 increased by a factor of 6. Conversely, a decrease of 5% of $[NaClO_2]$ resulted in the total disappearence of the uniform region; then the whole disc surgace was covered with patterns.

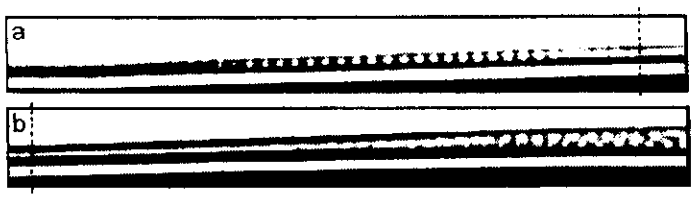

Fig. 5. Transient situation in the bevelled thin strip. The whole sequence can be reconstructed by placing side by side images (a) and (b). The vertical dotted lines indicate the same location along the strip. Note that the symmetry breaking pattern has disappeared over large lumps of the reactor. Picture taken 2 h after a 10% increase in the chlorite concentration. All other experimental conditions as in Fig. 2.

3.2. *Transient situation*

Asymptotic states as those presented above, in Figs. 2 and 3, are reached after about 10 h. Before this time, some remarkable transient situations can be observed, either when a new experiment is started or after a jump in the value of some chemical constraint during a series of experiments. In the latter case, the initial symmetry breaking patterns are erased over more or less extended parts of the gel reactors. In Sections 3.2.1 and 3.2.2, we shall examine transient situations observed after a 10% increase in the chlorite concentration.

3.2.1. *In bevelled thin strip*

Fig. 5 shows a transient situation in the bevelled gel strip. The symmetry breaking pattern was completely erased (see right end of Fig. 5(a) and left end of Fig. 5(b)) over a large extent comprised between the region with one row of spots (Fig. 5(a)) and the transition region (right end of Fig. 5(b)). At both ends of this now uniform clear band, patterns are similar to those observed in the initial asymptotic state. After this transient situation, the system evolves towards a new asymptotic state: spots slowly reinvade this temporally featureless band while, at the other end of the row, spots disappear and the region without symmetry breaking pattern gains in extension in the narrowest parts of the bevelled strip.

3.2.2. *In bevelled disc*

An equivalent transient situation is observed in the bevelled disc reactor, Fig. 6. The patterns in regions 3 and 4 are transiently erased. Then during the evolution towards the new steady state, stripes progressively reinvade this temporary uniform region. However, the expanding stripe region is preceded by a region tesselated with hexagonal arrays of dark spots. This remarkable new hexagonal patterns could never be stabilized in any of the tested asymptotic states. Note that these patterns are relatively long-lived since they have been observed for about 8 h. Ultimately, the stripe structure spreads over the whole area, and a pattern sequence similar to that of Fig. 3 is recovered.

4. Discussion

It is worth noting that, in the thin strip reactor, essentially one type of symmetry breaking pattern is observed, i.e. spots arranged in rows parallel to the feed boundaries. However, in the transition region between one and two rows, there can be different stationary phase relations between the peaks in two rows. As already mentioned, in a very thin strip ($h \leq \lambda$), one row of spots can be thought as the experimental approximation of a one-dimensional Turing pattern. In a genuine uniformly constrained (theoretical) one-dimensional reaction – diffusion system, the only possible stationary symmetry breaking pattern is a periodic longitudinal amplitude modulation. In an ideally thin two-dimensional system with a strong parameter gradient in one direction, theoretical simulations show that the Turing pattern emerges as a single row of spots perpendicular to the gradient. This pattern is shown to have the same bifurcation properties as a one-dimensional system [9]. Our experiments are usually performed in gel strips with a thickness comparable to the wavelength of the pattern ($h \cong \lambda$). The observed

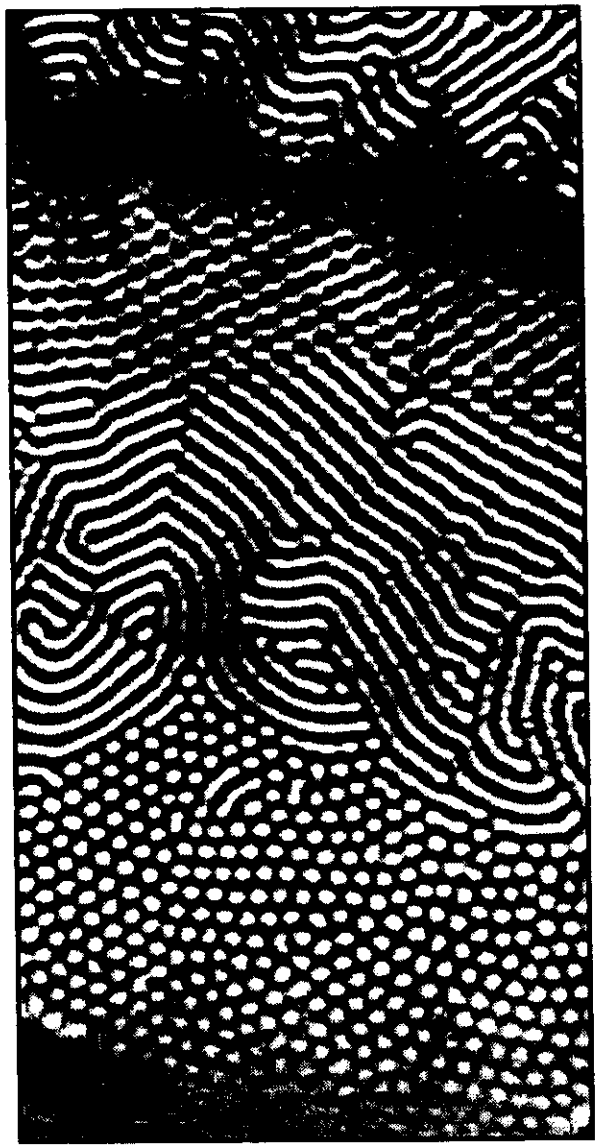

Fig. 6. Transient pattern sequence in the bevelled disc. Note that, as in Fig. 5, the pattern has disappeared over large extents; see the region of homogeneous state located in the upper parts of the figure; see also the black hexagons at the borders of this region. Picture taken 2 h after 10% increase in the chlorite concentration. All other experimental conditions as in Fig. 3.

"quasi-one-dimensional" pattern can actually be made either of short columns perpendicular to the observation plane or of beads, and no distinction can be made between a column and a bead pattern. However, as we have mentioned, in the widest parts of the bevelled gel strip, at some places, spots inside one row become fuzzy or even disappear, giving place to segments of clear bands. Such segments can be understood as columns layed parallel to the impermeable boundaries. Another possibility is that, due to a difficult rearrangement of a number of spots emerging in a limited space inside the row, the corresponding zone in the pattern region exhibits a vanishing amplitude modulation. Such segments can be considered as defects of the pattern. The capability of the system to eliminate such defects seems very limited since these clear segments held unchanged for about two days, the usual duration of an experiment.

The diversity of patterns observed in the bevelled disc reactor will be better understood when comparing these observations with those made in the bevelled strip reactor at locations with comparable distances between the feed boundaries. We thus compare in the two reactors, locations with the same width of pattern-forming region. However, if the gel strip reactor provides information on the number of separated pattern layers, in any case it can provide information on the type of pattern selected in the layers that develop in the disc reactor.

In the thinnest region of the disc as in the narrowest part of the strip, no symmetry breaking pattern develops. The region of the gel strip where pattern is made of one row of spots fits regions 2 and 3 in the disc over which hexagonal arrays of clear spots and stripe patterns can be seen. Thus, these patterns correspond to genuine monolayer patterns. In these monolayers, the spot and stripe patterns actually correspond, respectively, to bead and column structures. Note that these columns are seldom straight but generally bent columns. In the following, they will be simply referred as "columns". The spot and stripe patterns in regions 2 and 3 of the disc are characterized by their relative sharpness. Such hexagon and stripe patterns have initially been observed by Ouyang and Swinney [17,18] and later by others [23] and thought as effective quasi-two-dimensional patterns. It has been shown theoretically that, at onset, monolayers of Turing patterns have the same qualitative bifurcation diagram and pattern selection properties than two-dimensional systems [7,9]. The hexagonal mode is generally the

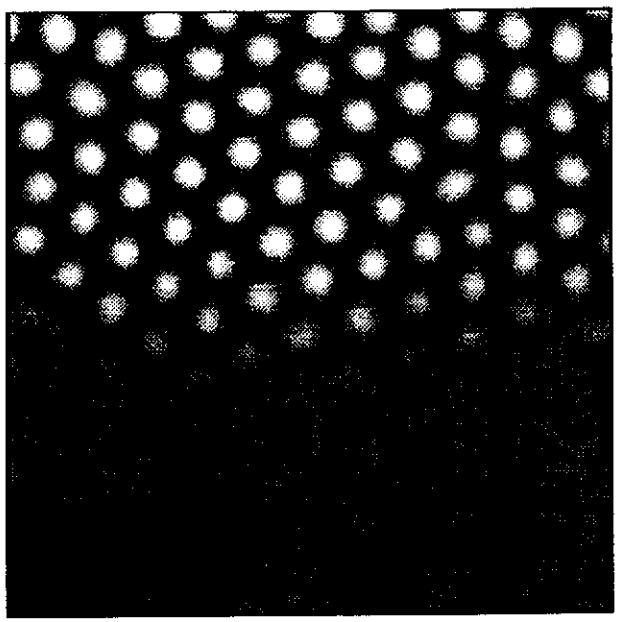

Fig. 7. The transition between the domains of uniform state and hexagon pattern. Magnification of a small region.

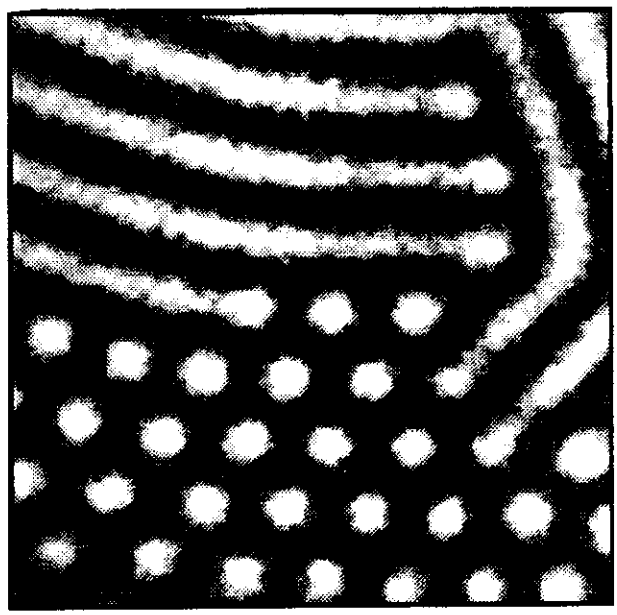

Fig. 8. The transition between the domains of hexagon and stripe patterns. Magnification of a small region.

first stable mode and appears subcritically; the stripe mode becomes stable only at some distance from onset while hexagons loose their stability. The stability domains of these two modes overlap over some range of bifurcation parameter values. However, there is an important difference between genuine two-dimensional systems and monolayers: in the latter, the hexagonal mode is generically restabilized at some distance from onset [7,9]. Note that the sequence uniform–hexagons–stripes experimentally observed in the bevelled disc, follows exactly the stability order predicted by the linear stability analysis. In the asymptotic state we usually observe a very sharp transition between the uniform state and the hexagon pattern, i.e. the amplitude suddenly damps within a wavelength (see Fig. 7) which is consistent with the subcritical nature of the bifurcation to hexagons. However, we have never observed any obvious hysteresis in the position of this transition front as a function of feed parameters. Such hysteresis could be expected as a result of a front pinning due to non-variational effects. The same sharp transition is observed between hexagon (region 2) and stripe (region 3) patterns (see Fig. 8). No mixed state is observed at this front. This is consistent with the discontinuous nature of the transition between the stable hexagonal and striped modes. Here again no noticeable hysteresis is found as a function of constraints, contrary to another report [21]. No pinning is observed in our experimental conditions which infers a weak overlap of the stability domains of hexagons and stripes.

The intricate pattern in region 4 is made of modulated stripes and it is very tempting to think of this pattern as a mixed mode. However, in the classical two-dimensional approach, this mixed mode is unstable [31]. The modulated stripes of region 4 develop in the continuation of the regular stripes of region 3. Modulations are regularly spaced along the stripes and form a hexagonal array of higher light intensity. Region 4 in the bevelled disc of gel would correspond to the transition region where a second row of spots is seen to progressively emerge in the bevelled strip. This occurs when the width Δ of the pattern-forming region exceeds a critical size. Region 4 in the disc can be understood as a region where a second layer of pattern is building up; a truely three-dimensional pattern is unfolding here. Fig. 9 provides a magnification of the transition region between regions 3 and 4: At the frontier with region 3, spots are few and have

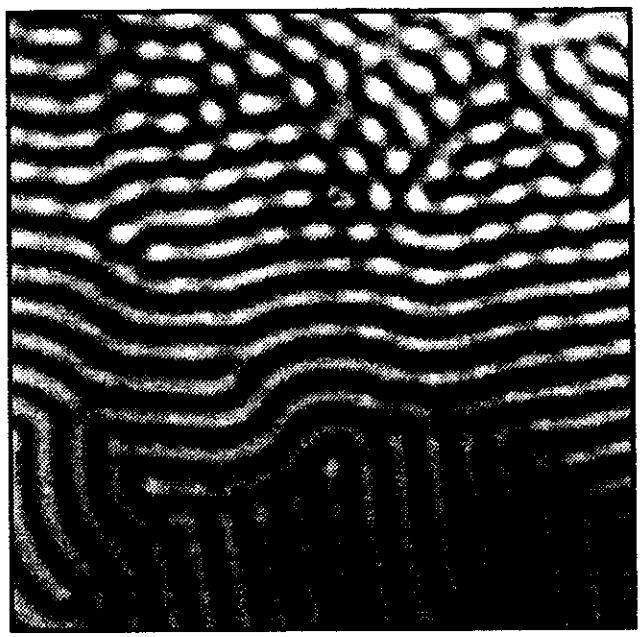

Fig. 9. Detailed view of the transition zone between regions 3 and 4. Note the hexagon–stripe mixed pattern.

a low amplitude. Going upwards, towards region 5, spots along the stripes become more numerous and regularly spaced. In the light of our observations in the gel strip, we conjecture that these spots develop as outgrowths on the columnar structure of the first pattern layer. Note that the spots stay basically centred along the clear columns.

Subsequently, with the increased thickness of the disc of gel, outgrowths would form an extra roll along the initial columns, so that we can understand the structure in region 5 as being formed of two layers of parallel columns. Region 5 in the disc corresponds in the gel strip to the regions with two rows of spots either with a slight shift between splitting pairs or completely staggered spots. Generally, in region 5, the columns of the second layer do not settle at equal distance from two neighbour columns in the first layer but rather stay closer to one of them. The projection of such a three-dimensional arrangement on the plane of the picture results in a pattern made of stripes with poorer constrast than in region 3. A magnification of such a picture with enhanced constrast is given in Fig. 10 with the light intensity profile taken along a line perpendicular to the direction of the stripes. The profile shows a period made of two peaks with two unequal heights. This can be understood as the superposition of two non-harmonic modulations of the light intensity. Note that non-harmonic modulations are generally expected far from onset. The non-symmetric shape of the profile could result either from a phase shift actually slightly less than half a wavelength between the columns in the two layers (as suggested also by the observations in the bevelled strip reactor) or from a bias in the observation direction of a symmetric array of staggered columns. Our observations in the strip reactor seem to favour the first assumption.

Thus, we have observed the emergence of a second layer of pattern which, in region 4, is made of a hexagonal array of beads more or less separated from the columns of the first pattern layer; these beads transform into parallel columns in region 5 and the sequence hexagon–stripe experimentally observed for the first layer repeats in the second one. This means that various layers of patterns can develop at different distances from the feed boundaries, and each layer can undergo, somewhat independently, the same pattern

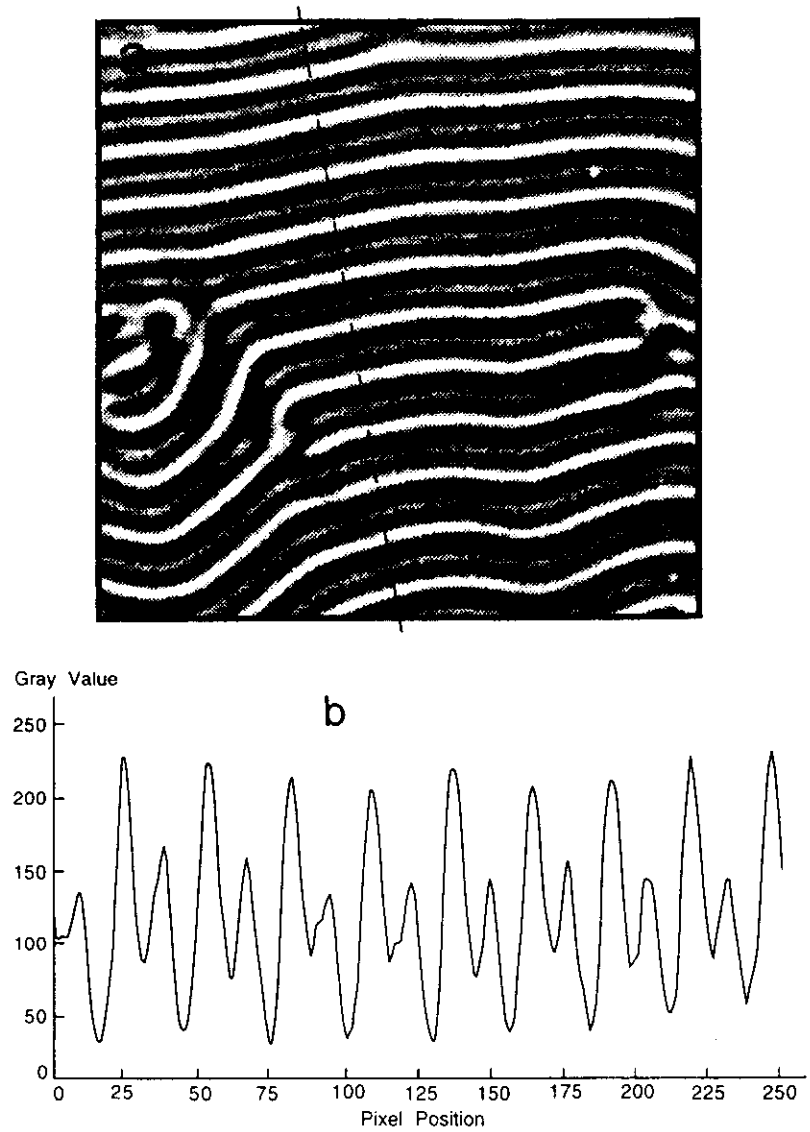

Fig. 10. The asymmetric stripes of region 5: (a) a magnification; (b) the light intensity profile along the line (-------) drawn in picture (a).

mode sequence as the thickness of the disc reactor increases. Moreover, different planforms can be observed at a given disc thickness, in adjacent layers. This is in agreement with preliminary theoretical [24] as well as experimental [21] results obtained in three-dimensional systems in the presence of parameter gradients.

At first glance, region 6 exhibits a wealth of very intricate planforms. However, a closer examination of these apparently different planforms brings the conclusion that they are various aspects of the same basic organization. Such patterns typically appear as illustrated in Fig. 11. Planforms of this type are observed at the top of the disc, as in Fig. 3. Such regions of the bevelled disc correspond to regions of the bevelled strip where the pattern is made of two rows of spots; so that the planform of Fig. 11 can be considered as the projection on the observation plane of two patterns

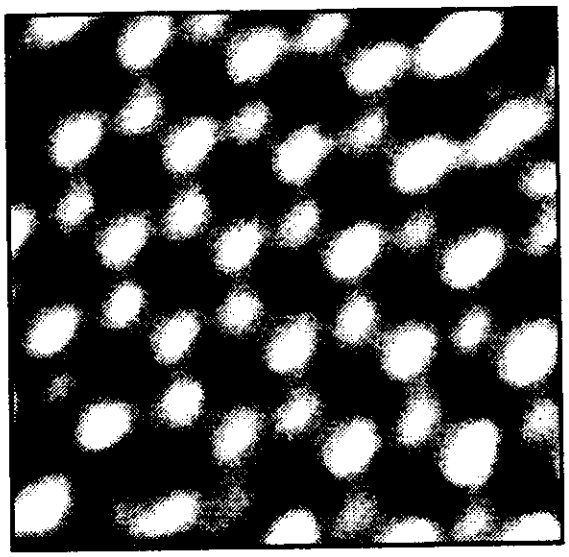

Fig. 11. An example of intricate planform commonly observed in region 6.

that develop in two adjacent layers. Such non-standard planforms are rather difficult to elucidate. They can be understood as moiré images of standard planforms. Patterns very similar to those of region 6 can be obtained by summing an image of hexagonal array of clear spots and an image of stripes from regions 2 and 3, with the clear spots superposed to the dark stripes. Note the necessary phase shift of π compared to the superposition that produces planforms such as those observed in region 4. This superposition of spots and stripes in region 6 implies that a spot pattern is restabilized in the top of the disc reactor, Such a restabilization of the hexagonal mode is also found in many computations and analytical calculations on the Brusselator [7,32] and the Schnackenberg [8,9] models. This phenomen is often referred as reentrance.

Another case of reentrance is obtained in the transient shown in Fig. 6 which exhibits the sequence uniform – clear hexagons – stripes – dark hexagons – uniform. This can be thought as two different Turing bifurcations from uniform to hexagons, one of them from uniform to clear hexagons, and the other from uniform to dark hexagons. This can be theoretically understood if the quadratic term of the normal form of the Turing bifurcation changes sign. Note that dark hexagons have always been observed as transient in experiments. It is also remarkable that dark spots were never observed in the bevelled strip, even transiently.

Let us now consider again the uniform state next to the dark hexagons. This region has to be associated to the temporary featureless clear band in the strip reactor (Fig. 5). In the disc reactor, this should then correspond to a clear sheet which could constitute the first element of a lamellar structure predicted by theory in three-dimensional systems [10]. As the black hexagons, this structure is unstable under our experimental conditions.

5. Conclusion

We have used an indirect approach in order to address the problem of the actual pattern organization in three-dimensional systems, in the presence of feed gradients. Indeed, there is a severe technical obstacle to the direct analysis of three-dimensional structures: the structures correspond to smooth continuous changes in concentration of diluted species and the contrast of patterns decreases with the decrease of the focal depth. The direct analysis would call for focal depth much smaller than the wavelength of the pattern, that is of the order of a few hundredth of millimeter; in these conditions, contrast would be so low that very low noise camera and frame average techniques should be used much in the same way as in confocal microscopy. Other authors seem to have made a rough measurement of the thickness and position of the pattern-forming region [33]. However, as mentioned by these authors, the accuracy of their method heavily depends on the pattern contrast which can decrease from one layer to the next, making difficult the actual determination of the number of layers.

Our innovative approach consisted in designing reactors that enable to slowly unfold the pattern transitions along one direction of the reactors. These reactors can be thought of as the non-linear chemistry analogues of the Kofler hot stage used in the determination of equilibrium phase transitions. In our reactors, the uniform–hexagon–stripe transition sequence classically predicted in theoretical studies, was directly viewed, unfolded in space. The continous

follow up of pattern evolution allowed us to draw some conclusions on bilayer patterns. In particular, we have been able to follow the emergence of a bilayer from a monolayer pattern and have shown that this transition is progressive.

The presence of steep feed gradients seems to make the three-dimensional pattern selection mechanism resourceful through the coupling of basic patterns. In our experiments these are the basic two-dimensional hexagonal and stripe modes. The main question which is still to be solved is that of the determination of the possible stable phase relations that can exist between the patterns in the two layers. Our observations suggest that several such phase shifts are possible and that the relative stability of these phase relations may depend on the constraints and probably on the exact shape of the confining parameter well. However, the method becomes unreliable for more than two patterned planes.

Note that in this series of experiments, we have not identified patterns that could result from the superposition of two layers of hexagons. However, triangular patterns observed in other experiments [34] suggest that the superposition of a clear and a dark hexagon layers is possible. Refined experiments with our bevelled reactors are now in progress. Moreover in new sets of experiments, the spatio-temporal behaviours [23] that result from the superposition of a temporal instability (Hopf) in one plane and a spatial instability (Turing) in another are distinguished from behaviours that develop in a single stratum of width Δ comparable to the Turing wavelength λ. This will be the subject of a forthcoming paper.

Acknowledgements

The authors are indebted to Dr. Jacques Boissonade for stimulating discussions and for sharing the results of his numerical simulations prior to publication.

References

[1] V. Castets, E. Dulos, J. Boissonade and P. De Kepper, Phys. Rev. Lett. 64 (1990) 2953.
[2] A.M. Turing, Philos. Trans. Roy. Soc. London B 327 (1952) 37.
[3] G. Nicolis and I. Prigogine, Self Organization in Nonequilibrium Chemical Systems (Wiley, New York, 1977).
[4] J.D. Murray, Mathematical Biology (Springer, Berlin, 1989).
[5] H. Meinhardt, Models of Biological Pattern Formation (Academic Press, New York, 1982).
[6] L.G. Harrison, Int. J. Plant Sci. 153 (1992) S76.
[7] P. Borckmans, A. De Wit and G. Dewel, Physica A 188 (1992) 137.
[8] V. Dufiet and J. Boissonade, J. Chem. Phys. 96 (1992) 664.
[9] V. Dufiet and J. Boissonade, Physica A 188 (1992) 158.
[10] A. De Wit, G. Dewel, P. Borckmans and D. Walgraef, Physica D 61 (1992) 289.
[11] M. Herschkowitz-Kaufman and G. Nicolis, J. Chem. Phys. 56 (1972) 1980; J.F. Auchmuty and G. Nicolis, Bull. Math. Biol. 37 (1975) 323.
[12] T.C. Lacalli, D.A. Wilkinson and L.G. Harrison, Development 104 (1988) 105.
[13] A. Hunding and M. Brons, Physica D 44 (1990) 285.
[14] J. Boissonade, J. Physique (France) 49 (1988) 541.
[15] P. De Kepper, V. Castets, E. Dulos and J. Boissonade, Physica D 49 (1991) 161.
[16] J. Boissonade, V. Castets, E. Dulos and P. De Kepper, Int. Ser. Num. Math. 97 (1991) 67.
[17] Q. Ouyang and H.L. Swinney, Nature 352 (1991) 610.
[18] Q. Ouyang and H.L. Swinney, Chaos 1 (1991) 411.
[19] J.J. Perraud, K. Agladze, E. Dulos and P. De Kepper, Physica A 188 (1992) 1.
[20] R.D. Vigil, Q. Ouyang and H.L. Swinney, Physica A 188 (1992) 17.
[21] Q. Ouyang, Z. Noszticzius and H.L. Swinney, J. Chem. Phys. 96 (1992) 6773.
[22] K.L. Lee, Q. Ouyang, W.D. McCormick and H.L. Swinney, preprint.
[23] P. De Kepper, J.J. Perraud, B. Rudovics and E. Dulos, Int. J. Bif. Chaos 4 (1994) 1215.
[24] J. Boissonade, E. Dulos and P. De Kepper, in: Chemical Waves and Patterns, eds. R. Kapral and K. Schowalter (Kluwer Academic Publishers, Dordrecht, 1995) 221.
[25] Z. Noszticzius, Q. Ouyang, W.D. McCormick and H.L. Swinney, J. Chem. Phys. 96 (1992) 6302.
[26] P. De Kepper, I.R. Epstein, K. Kustin and M. Orbán, J. Phys. Chem. 86 (1982) 170.
[27] I. Lengyel and I.R. Epstein, Science 251 (1990) 650.
[28] I. Lengyel and I.R. Epstein, Proc. Nat. Acad. Sci. USA 89 (1992) 3977.
[29] J.E. Pearson and N.J. Bruno, Chaos 2 (1992) 513.
[30] K. Agladze, E. Dulos and P. De Kepper, J. Phys. Chem. 96 (1992) 2400.
[31] A. De Wit, G. Dewel and P. Borckmans, Phys. Rev. E 48 (1993) R4191.
[32] G. Dewel, P. Borckmans, A. De Wit, B. Rudovics, J.J. Perraud, E. Dulos, J. Boissonade and P. De Kepper, Physica A 213 (1995) 181.
[33] I. Lengyel, S. Kádár and I.R. Epstein, Phys. Rev. Lett. 69 (1992) 2729.
[34] B. Rudovics, Ph.D. Thesis, Bordeaux, France (1995).

Dynamics of Turing pattern monolayers close to onset

V. Dufiet and J. Boissonade
Centre de Recherche Paul Pascal, CNRS Bordeaux, Avenue Schweitzer, F-33600 Pessac, France
(Received 27 February 1995)

We perform simulations of Turing patterns confined to a monolayer by a gradient of parameters in a three-dimensional system. The results provide a more comprehensive basis for the interpretation of the actual experimental results than the usual, but disputable, interpretation in terms of ideal two-dimensional systems. Systematic comparison of the bifurcation behavior in genuine two-dimensional systems and in such monolayers is achieved with a theoretical model. We show that in the monolayers, hexagonal phases are restabilized as a result of the longitudinal instability. [S1063-651X(96)09905-9]

PACS number(s): 47.54.+r, 05.70.Ln, 82.20.Mj, 82.20.Wt

I. INTRODUCTION

Turing structures are self-organized stationary concentration patterns which result from the sole competition between reaction and diffusion in a class of chemical systems kept far from equilibrium by a permanent feed of fresh reactants. These chemical systems must exhibit the following features. First, the reaction kinetics is controlled by two antagonistic feedback loops, namely, an activation process—such as an autocatalytic reaction—and an inhibitory process. This set of properties is common to various types of "active media" that exhibit exotic temporal or spatial behavior, like multistability, periodic or chaotic oscillations, excitability, or wave propagation [1–5]. For Turing patterns to form, a species controlling the inhibitory process must diffuse much faster than any species controlling the activation process. First predicted in 1952 [6], they have been thoroughly investigated from a theoretical point of view (for reviews see Refs. [1, 4, 7]). Nevertheless, almost 40 years passed before they were experimentally evidenced with the so-called chlorite-iodine-malonic acid (CIMA) reaction [8], first in a gel strip reactor [9–11], then in a gel disk reactor [12,13]. The latter setup has become the most commonly used. It is made of a thin flat piece of gel with two opposite faces kept in contact with permanently refreshed reservoirs of different input solutions. The input species diffuse from the reservoirs into the gel where they meet and react. A gradient of the input reactants concentrations spontaneously develops in the direction orthogonal to the faces, establishing a continuous change of control parameters. A pattern, breaking the planar symmetry, will form in regions where the values of these local parameters meet the conditions for a Turing instability, i.e., in a thick stratum parallel to the faces (Fig. 1) [14]. In the actual experiments, the width of this stratum commonly reaches three or four wavelengths [15]. Thus—contrary to the well-known Rayleigh-Bénard convective structures—they present a three-dimensional character. The patterns are normally looked at in a direction parallel to the gradient, so that the light absorption is averaged over the film thickness and there is some uncertainty on the true geometry of the structures. Nevertheless, when a control parameter is changed continuously, the width of the unstable region grows progressively. The structures are thus found to form one layer after the other, so that just beyond the pattern onset there is a single layer [16]. We shall call this type of pattern a "monolayer." Transverse dimensions of reactors are large enough (more than 100 wavelengths) for the boundary effects to be negligible and these patterns are generally coherent and quite periodic over large size domains separated by topological defects. In these conditions, the most common regular planforms observed through the gel are stripes or hexagons. In regard of their quasi-two-dimensional character and the analogies in planforms, pattern selection theories developed for genuine two-dimensional (2D) system are commonly applied to the experimental monolayers.

Unfortunately, there is no definite evidence that the selection stability properties are identical in these genuine 2D patterns and in those restricted to a single layer bounded by a strong gradient of control parameters. There has been a number of analytical and numerical studies of patterns in a ramp of control parameters [11,17–27]. None of them really meet the requirements above. Analytical methods generally rely on slow parameter ramps in contradiction with such strong localization problems. Two-dimensional systems with parameter ramps may exhibit patterns made of a single row of dots, the 1D analog of the 2D monolayers [11,21], but this problem turns out to be of a different kind due to the nonexistence of rotational invariance in one dimension.

In order to clarify the relations between the genuine homogeneous 2D systems and the monolayers, we have studied the selection of patterns close to onset for the same model in both geometries. In Sec. II, we introduce a simple appropriate reaction-diffusion model that exhibits Turing patterns. Then we study the selection of patterns close to onset and check the numerical results with those predicted from a weakly nonlinear analysis. In Sec. III, we mimic a disk reactor by introducing a parameter ramp that induces the formation of monolayers in agreement with the experimental observations. On the basis of 3D numerical simulations we show that a transverse instability leading to the formation of a monolayer precedes a longitudinal instability. We show that, very close to onset, the monolayers behave like genuine 2D systems but that, in relation with the longitudinal instability, hexagonal phases are restabilized when the distance to threshold increases. This property is interpreted as a result of the coupling of the cubic terms with a homogeneous mode, in agreement with the recent theory of Price [28].

In the following, we call "2D systems" without further precision genuine two-dimensional systems with uniform control parameters. We always consider the relative stability

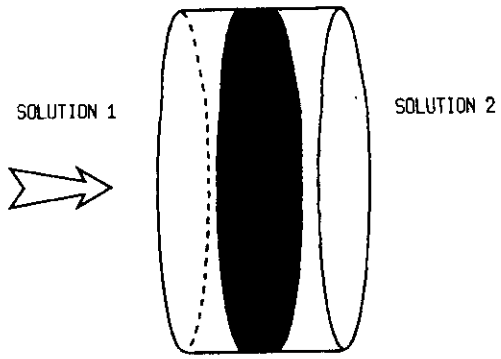

FIG. 1. Scheme of a disk reactor. Input reactants are provided by solutions 1 and 2. Structures form in the gray region. The arrow indicates the direction of observation.

of regular periodic patterns—stripes or hexagons patterns—without topological defects and assume periodic boundary conditions in the pattern plane. All 2D and 3D computations were performed with an implicit hopscotch method [29] tailored to handle the nonlinear terms [30].

II. TWO-DIMENSIONAL SYSTEMS

In order to make clear the comparison with the monolayers, we shall report rather extensively the analytical and numerical properties of the two-dimensional systems that will be used as a reference in Sec. III.

A. Reaction-diffusion model

The linearization around the stationary state of any two-variable reaction-diffusion system able to exhibit Turing patterns can always be written in the form

$$\frac{\partial u}{\partial t}=a_1 u-\eta a_2 v+D_u\nabla^2 u,$$

$$\frac{\partial v}{\partial t}=\eta a_3 u-a_4 v+D_v\nabla^2 v, \tag{1}$$

where $a_i>0$, $\eta=\pm 1$, and D_u and D_v are the diffusion coefficients [4,31,32]. The model is called *activator-inhibitor* if $\eta=+1$ and *substrate-depleted* if $\eta=-1$. The number of coefficients can be reduced to three for each type of model by rescaling the concentrations, the time, and the space coordinates. Without lack of generality, we can restrict ourself to the activator-inhibitor type. Introducing the ratio $d=D_v/D_u$, a convenient form of the rescaled system is

$$\frac{\partial u}{\partial t}=u-\alpha v+\nabla^2 u,$$

$$\frac{\partial v}{\partial t}=u-\beta v+d\nabla^2 v, \tag{2}$$

with $\alpha>0$ and $\beta>0$. Variable u is the activator, whereas v is the inhibitor.

One can define a reaction-diffusion system that give rise to Turing patterns by adding a minimum of nonlinear terms to this set of equations:

$$\frac{\partial u}{\partial t}=u-\alpha v+\gamma uv-u^3+\nabla^2 u,$$

$$\frac{\partial v}{\partial t}=u-\beta v+d\nabla^2 v. \tag{3}$$

The cubic term $-u^3$ limits the exponential growth of the perturbation and allows for the saturation of the instability. The quadratic term γuv avoids the invariance in the transformation $(u,v)\rightarrow(-u,-v)$, which is nongeneric in chemical systems. This particular symmetry can be restored by setting $\gamma=0$. Although this model has not been derived from a chemical scheme, it exhibits the same properties and has been preferred in regard of its simplest analytical properties.

This model has a uniform stationary state $(u=v=0)$ independent of the control parameters α, β, γ, d. The linear stability analysis of this stationary state—hereafter referred as the "zero" state—follows from the linearization of system (3) which actually reduces to Eqs. (2). In the absence of diffusion, the homogeneous system exhibits a Hopf bifurcation at $\beta=1$ (when $\alpha>1$) and an exchange of stability or a pitchfork bifurcation along the line $\alpha=\beta$. The stationary state is stable to any small homogeneous perturbation for $1<\beta<\alpha$ (Fig. 2). When the diffusion terms are present, the stationary state can become unstable, in this parameter domain, to a nonuniform perturbation $\mathbf{u}=\mathbf{u}_0\exp(i\mathbf{k}\cdot\mathbf{r})$ of wave vector $\mathbf{k}\neq\mathbf{0}$, where $\mathbf{u}=\binom{u_1}{v_1}$. This Turing bifurcation occurs when the real part of an eigenvalue of the linear operator

$$L=\begin{pmatrix}1-k^2 & -\alpha\\ 1 & -\beta-dk^2\end{pmatrix} \tag{4}$$

becomes positive, that is, when the determinant Δ and the first derivative $d\Delta/dk$ are simultaneously zero. The Turing bifurcation is located along the line AB (Fig. 2) defined by the equation

$$\alpha=\alpha_c=\frac{(\beta+d)^2}{4d}. \tag{5}$$

The critical wavenumber k_c is given by

$$k_c^2=\frac{d-\beta}{2d}. \tag{6}$$

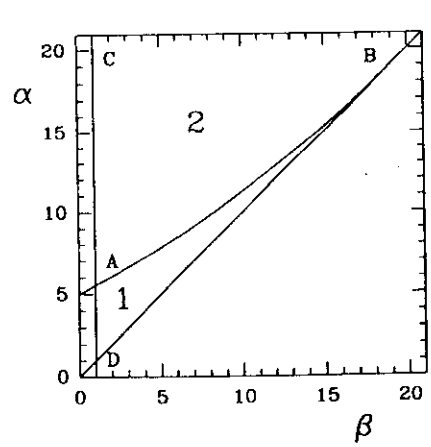

FIG. 2. Bifurcation diagram at $d=20$. (1) Turing space. (2) Stable stationnaire state ($\beta>1$). AB: limit of Turing bifurcation ($\beta<20$). CD: limit of Hopf bifurcation ($\alpha>1$).

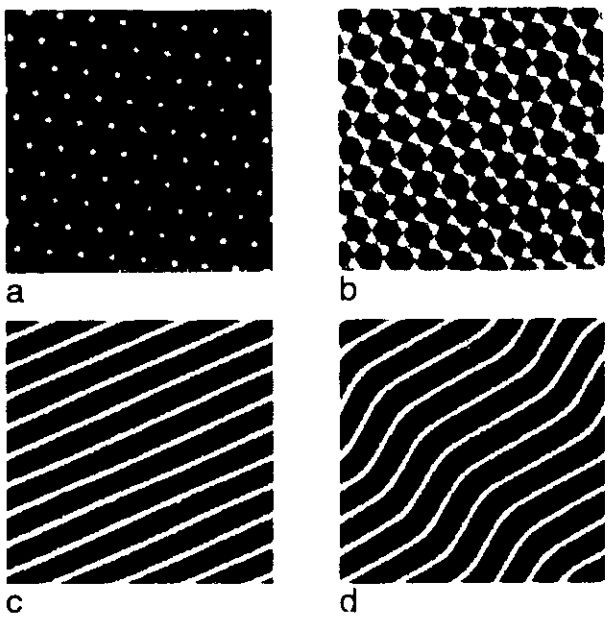

FIG. 3. Two-dimensional patterns. (a) hexagonal pattern H_0 ($\alpha=7.81$, $\beta=5$, $\gamma=0.75$, $d=20$, size: 100×100); (b) hexagonal pattern H_π ($\alpha=7.81$, $\beta=5$, $\gamma=0.75$, $d=20$, size: 100×100); (c) striped pattern ($\alpha=7.45$, $\beta=5$, $\gamma=1$, $d=20$, size: 100×100); (d) zigzag pattern ($\alpha=7.3$, $\beta=5$, $\gamma=1$, $d=20$, size: 100×100).

The parameter domain where the stationary state is unstable only to a nonuniform perturbation—sometimes called the "Turing space" [3]—is represented in Fig. 2. As expected, this domain exists only when the inhibitor species diffuses faster than the activator species and the area of this Turing space increases with the ratio d.

We shall now consider the formation and the selection of patterns close to the onset $\alpha=\alpha_c$—i.e., the line AB—and avoid as much as possible coupling with other instabilities, i.e., the vicinity of lines BD and CD.

If not otherwise stated, α is used as the expandable bifurcation parameter and the numerical simulations are carried out with the values $d=20$ and $\beta=5$. With this parameter set, the Turing bifurcation is located at $\alpha_c=7.8125$ and $k_c=0.6124$.

B. Weakly nonlinear theory and selection of patterns

Figure 3 illustrates the different types of stable stationary patterns that are found in numerical simulations when exploring the parameter space. The variable u is represented on a gray scale, changing from black (minimum value) to white (maximum value). The variable v changes in phase with u and exhibits similar patterns. When the patterns spontaneously emerge from a noisy initial unstable stationary state, they naturally contain topological defects that move and relax slowly. If the system is finite these defects tend to vanish on a long time scale. From now on, we shall consider only periodic patterns without topological defects. We also assume that they are stable to small charges of wavelength caused by cross-roll or phase instabilities [33].

All the patterns in Fig. 3 are made of stripes and hexagons. There are two types of hexagons, respectively referred to as H_0 and H_π, according to whether the minima or the maxima are disposed on the hexagonal lattice. Stripes can be straight lines or exhibit periodic undulations that result from a previous zigzag instability [34]. The latter still belong to the stripe pattern category. The planforms in Fig. 3 are identical to those observed with other chemical schemes, like the Schnackenberg model [35,36] or the Brussellator [37]. This supports the validity of this simplified model.

Close to onset, the eigenvalues associated to the critical modes are close to zero, so that they evolve on a long time scale, whereas the noncritical stable modes relax rapidly. The whole dynamics can be therefore reduced to the dynamics of the active slow modes, which slave the fast stable modes [2]. The stability and the selection of the different patterns close to onset can be derived from the amplitude equations that governs the dynamics of these active modes. Hexagonal and stripe patterns are thus well described by a system of three active resonant pairs of modes $(\mathbf{k}_i,-\mathbf{k}_i)_{i=1,2,3}$ making angles of $2\pi/3$.

Close to onset, the solutions are given by

$$\mathbf{u}=\mathbf{u}_0\cdot\sum_{\mathbf{k}_j}[A_j\exp(i\mathbf{k}_j\cdot\mathbf{r})+\mathbf{A}_j^*\exp(-i\mathbf{k}_j\cdot\mathbf{r})], \tag{7}$$

where $\mathbf{u}_0$ defines the direction of the eigenmodes in concentration space (i.e., the ratio u/v) and where A_j and the conjugate A_j^* are, respectively, the amplitude associated with modes $\mathbf{k}_j$ and $-\mathbf{k}_j$. From standard symmetry arguments, one can predict the general form of these amplitude equations at third order [38]:

$$\tau\frac{\partial A_1}{\partial t}=\mu A_1+\Gamma A_2^*A_3^*-[g|A_1|^2+g'(|A_2|^2+|A_3|^2)]A_1, \tag{8}$$

where $\mu=(\alpha_c-\alpha)/\alpha$ is a normalized distance to onset. Similar equations for A_2 and A_3 are obtained by circular permutation of indices. To avoid confusions, always keep in mind that, for model (3), the stationary state becomes Turing unstable when the bifurcation parameter α *decreases*, so that the distance to onset increases when the bifurcation parameter decreases.

The form of Eq. (8) is general for Turing bifurcations, but the exact expressions of the coefficients are specific to the model. Their derivation for our particular model (3) is reported in Ref. [30]. For amplitude of u, they are

$$\tau=\frac{2(d-1)}{\beta+d},\quad \Gamma=\frac{8d\gamma}{(\beta+d)^2}, \tag{9}$$

$$g=\frac{6d}{\beta+d}-\frac{16d^2\gamma^2(53\beta+23d)}{9(\beta-d)^2(\beta+d)^3}, \tag{10}$$

$$g'=\frac{12d}{\beta+d}-\frac{32d^2\gamma^2(3\beta+d)}{(\beta-d)^2(\beta+d)^3}.$$

For these amplitude equations to be valid, saturation of the instability must be achieved at third order. This condition is satisfied when

$$|\gamma|<\gamma_c=\frac{3\sqrt{3}(d^2-b^2)}{2\sqrt{2}[d(53\beta+23d]^{1/2}}. \tag{11}$$

For $\beta=5$ and $d=20$, $\gamma_c\approx5.721$, and the above conditions are satisfied for $|\gamma|=1$.

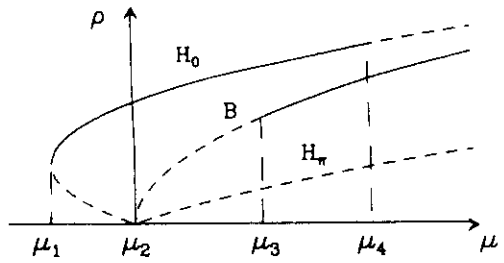

FIG. 4. Schematic bifurcation diagram for $\Gamma>0$. H_0: hexagonal patterns with $\Phi=0$; H_π: hexagonal patterns with $\Phi=\pi$; B: striped patterns; —: stable states, ---: unstable states. For $\Gamma<0$, the indices 0 and π must be exchanged.

Amplitudes in Eq. (8) can be written $A_j=\rho_j \exp \varphi_j$. It results from a standard stability analysis [26,38–40] that the only possible stable solutions are the steady state, a stripe pattern ($\rho_1\neq 0$, $\rho_2=\rho_3=0$) and the hexagonal patterns H_0 or H_π ($\rho_1=\rho_2=\rho_3$, with $\Phi=\varphi_1+\varphi_2+\varphi_3=0$ or π, respectively). Their existence and stability limits, as a function of the scaled bifurcation parameter μ, are ordered according to the scheme in Fig. 4 where the μ_i are given by

$$\mu_1=\frac{-\Gamma^2}{4(g+2g')}, \quad \mu_2=0,$$

$$\mu_3=\frac{\Gamma^2 g}{(g-g')^2}, \quad \mu_4=\frac{2g+g'}{(g'-g)^2}\Gamma^2. \tag{12}$$

Stable branches H_0 and H_π are mutually exclusive. The stable branch is H_0 if $\Gamma>0$ and H_π if $\Gamma<0$. A subcritical hexagonal branch comes out first at $\mu=\mu_1<0$ but loses stability when $\mu>\mu_4>0$. The supercritical stripe state branch is unstable close to the critical point but becomes stable for $\mu>\mu_3$. In the range $\mu_3<\mu<\mu_4$ both branches are stable. When $\gamma=0$ the nongeneric symmetry $(u,v)\rightarrow(-u,-v)$ is restored, one has $\Gamma=0$ and $\mu_1=\mu_2=\mu_3=\mu_4=0$. In this case, the stripe pattern bifurcates supercritically whereas the stability range of the hexagonal pattern vanishes. The latter is indeed directly related to the quadratic term Γ and proportional to γ^2 [41], in the model $\Gamma\propto\gamma$ so this stability range can be easily tuned.

The amplitude and stability of patterns obtained by direct numerical simulations and those obtained from the Eq. (8) are reported in Fig. 5 for $\gamma=0$ and $\gamma=0.75$ as a function of the distance to onset $\alpha_c-\alpha$. Close to onset, these results are in excellent agreement and confirm the validity of the approach.

When the nonlinear coefficients of the model also depend on the bifurcation parameter, the coefficients in Eq. (8) and the μ_i's may also depend on μ so that *one* of the hexagonal phases can regain stability at large μ. This direct reentrant phenomenon depends on the model and has been extensively discussed for the Brussellator [37] and for the Schnackenberg model [30,36]. Our model (3) avoids such a behavior that could bias the interpretation of results in Sec. III. However, Price has recently shown that hexagonal phases can be also restabilized—even in the absence of quadratic terms—if an active *homogeneous* mode, commonly referred as a d.c. mode, is present [28]. This can be found in particular when an homogeneous bifurcation occurs at some distance beyond

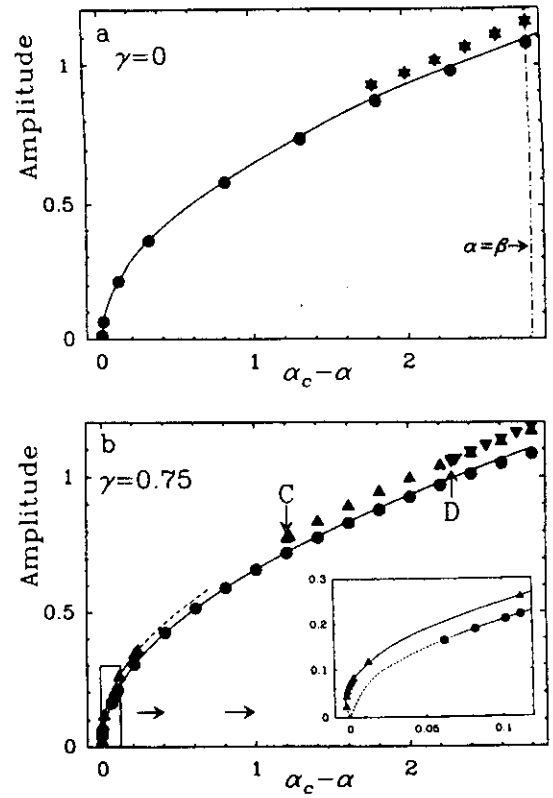

FIG. 5. Bifurcation diagrams of 2D system for model defined by Eqs. (3). ●: stable stripes, ▲: stable hexagons, H_0 (limit at C), ▼: stable hexagons H_π, (limit at D) (numerical simulation), —: stable states, ---: unstable states [computed from amplitude equations (8)–(10)]. (a) $\beta=5$, $\gamma=0$, $d=20$. (b) $\beta=5$, $\gamma=0.75$, $d=20$.

onset, as in our model at $\alpha=\beta$. In the vicinity of such bifurcations, the homogeneous mode becomes active and has to be included in the amplitude equations. Cubic interaction involving such an active mode of zero wave vector **0** generates in Eq. (8) a term of the form $A_0A_1^*A_2^*$. This term originates in the conservation law $\mathbf{k}_1=-\mathbf{k}_2-\mathbf{k}_3+\mathbf{0}$, where $(\mathbf{k}_1,\mathbf{k}_2,\mathbf{k}_3)$ is the basic triplet of the hexagonal structure. As it contains $A_2^*A_3^*$ like the quadratic term in Eq. (8), it plays the same stabilizing role for the hexagonal patterns. Nevertheless, if no other quadratic terms are present, H_0 and H_π are equivalent and are *both* restabilized. If there are quadratic terms in the dynamical equations [$\gamma\neq 0$ for model (3)], one of these pattern is favored and is restabilized first. This restabilization is shown in Fig. 5 for model (3) when α comes close to β. As expected, H_0 and H_π are both reentrant, at a common value $\alpha=\alpha_{R2}=6.02$ (i.e., $\alpha_c-\alpha_{R2}=1.7925$) for $\gamma=0$ [Fig. 5(a)], at different values for for $\gamma\neq 0$ [Fig. 5(b)]. In any case, the bifurcation scheme in Fig. 4 is preserved, provided that γ remains small enough. Note that since the wave vector of the faster growing mode gradually change with the distance to onset, the reentrant branches are actually only (re)stabilized for wave vectors slightly different of k_c. Those represented in Fig. 5 correspond to the wavevectors at which this restabilization occurs at the closest point to onset (respectively, $k_c\approx 0.55$ at $\gamma=0$ and $k_c\approx 0.57$ at $\gamma=0.75$). We shall see in Sec. III that the restabilization of hexagonal planforms by a d.c. mode can derive in a more indirect way from a different type of bifurcation.

III. MONOLAYERS

A. Monolayer modeling

We shall mimic the behavior of the experimental three dimensional disk reactors by introducing permanent gradients of at least one of the bifurcation parameters. In real disk reactors the input species concentrations are actually kept constant only on the feed surfaces but their gradients inside the gel are controlled both by diffusion and reaction. Thus, there is a feedback on the control parameters so that they are dynamical variables of the problem. Although such feedbacks can be incorporated in theoretical calculations [21], they depend on the specific form of the model. Nevertheless, in many cases, the reaction dynamics can be described by reduced models in which the control parameters are not the concentrations of input species themselves, but are effective constants, obtained by adiabatic eliminations or approximations on numerous variables. The experimental control parameters enter the equations through these constants. For instance, some of these species can be precursors that produce intermediate species at rates depending mainly on the input concentrations (a formal example is the Schnackenberg model [11]). Close to onset, supercritical Turing structures correspond to small amplitude spatial oscillations around the unstable stationary state. These small modulations are generally smoothed out and averaged in the feedback. In practice, one can thus assume that the spatial profiles of the control parameters are not coupled to these small variations of concentrations. For example, Lengyel and Epstein have proposed a satisfactory model of the (ClO_2-I^--malonic acid) reaction, a variant of the CIMA reaction which is also known to give Turing patterns [42]. They have shown that the whole set of reactions can be approximated by a two-variable model in a large range of parameters. The control parameters only depend on the feed concentrations and on the distance to the feed surfaces. They can be tuned independently in order that the system become supercritical in a layer parallel to the faces [14], i.e., the conditions expected to produce monolayers. Although the extension of these conclusions to the CIMA reaction or other models is not straightforward, modeling monolayers by introducing a tunable parameter profile appears to be a sound approach. The exact form of the model and of this profile do not seem critical for the conclusions that we shall draw in Sec. IV, provided that a few prerequisites accounting for experimental conditions are met.

In agreement with Sec. I, the following requirements must be retained: (a) The control parameter in the reaction-diffusion equations, say, α in Eq. (3), must change continuously along the sole direction $\mathbf{O}_z$, orthogonal to the opposite faces, and remain uniform in directions $\mathbf{O}_x$ and $\mathbf{O}_y$, parallel to these faces. (b) The profile of this primary parameter must be controlled through one (or several) tunable secondary control parameters that play the role of the tunable experimental constraints. (c) The primary control parameter must be subcritical on the faces (at $z=0$ and $z=L$) and take supercritical values over a range ΔL located at some distance from these faces. In the explored range of tunable parameters, ΔL must grow from zero to $\Delta L \sim \lambda$, in order to go from a uniform state to a structure extending over at least one wavelength along the direction $\mathbf{O}_z$. When ΔL further grows, multilayer structures settle. Such structures are beyond the scope of this paper.

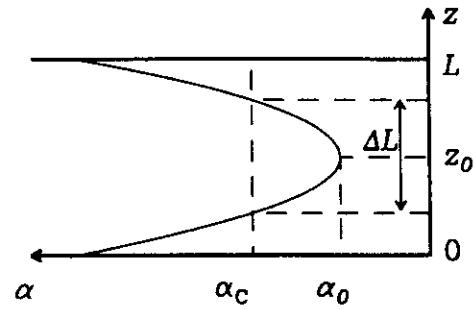

FIG. 6. Control parameter profile.

So far, there is no conclusive experimental argument to chose a particular parameter profile meeting these conditions. Thus we have retained a simple form, that is, a parabolic profile centered on the median plane $z=\frac{1}{2}L$. *A priori*, this gradient could be applied to any coefficient of the linearized equations. Since the different coefficients of the linearized equations [before scaling in order to keep all of them; see Eq. (1)] play different roles in the dynamics, one could expect that the properties depend of the choice of the coefficient on which the gradient is applied. Whichever coefficient is concerned, the results actually happen to be similar. This point will be briefly checked at the end of this section. The results extensively reported in this section have been obtained with the model (3) with the following spatial control parameter profile:

$$\alpha(z)=\alpha_0+\rho(z-z_0)^2. \tag{13}$$

Parameter ρ was kept fixed in each series of numerical experiments whereas α_0 was used as the tunable parameter. The function $\alpha(z)$ is maximum in the median plane $z=z_0=L/2$, where $\alpha(z)=\alpha_0$—the most supercritical value—and define a supercritical domain ΔL, where $\alpha(z)<\alpha_c$ centered on this median plane (Fig. 6). When comparing bifurcation diagrams of the 2D uniform systems of Sec. II with those of these 3D gradient systems, it is natural to use respectively α and α_0, or the distances to onset $\Delta\alpha=\alpha_c-\alpha$ and $\Delta\alpha_0=\alpha_{c0}-\alpha_0$.

Since the zero stationary state of our particular model is independent of the primary parameter α, the spatial organization results unambiguously from the Turing instability and cannot be confused with trivial spatial changes of the stationary state.

Two types of instabilities may occur according to the orientation of the wave vector.

A longitudinal instability, if the critical wave vector noted $\mathbf{k}_\parallel$, is oriented parallel to the gradient (orthogonal to the faces). The critical parameter can be determined in a 1D system colinear to the parameter gradient since, in this case, it is the only possible instability.

A transverse instability, if the critical wave vector noted $\mathbf{k}_\perp$, is oriented orthogonal to the gradient (parallel to the faces). This transverse mode is rotationally invariant in planes parallel to the faces. When a monolayer is considered as a 2D system, the wave vector $\mathbf{k}_\perp$ matches with $\mathbf{k}$.

Section III B is devoted to the determination of the first linear instability leading to a Turing structure and the form

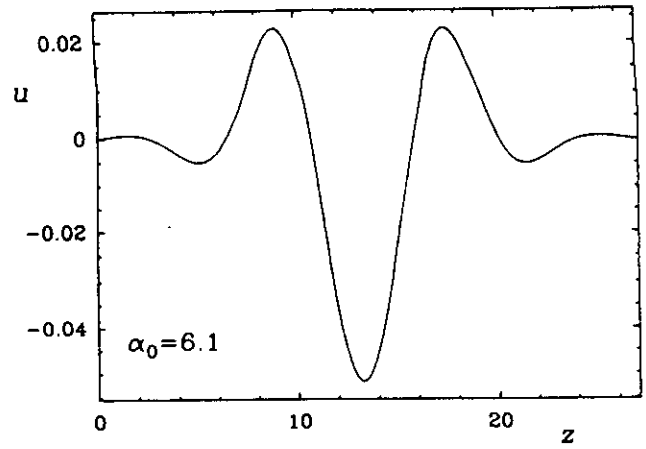

FIG. 7. Concentration profile $u(z)$ in the 1D system. $\alpha_0=6.1$, $\rho=0.15$, $\beta=5$, $\gamma=1$, $d=20$.

of the dispersion curve in the 3D systems described above. In Sec. III C, we report the bifurcation diagrams close to onset and the relative stability of the different patterns. These numerical results are compared to those obtained in Sec. II for genuine 2D systems and we discuss the limits of the concept of "monolayer." From now on, fixed parameters are given the following values: $\beta=5$, $d=20$, $\rho=0.15$. The linear properties are independent of the parameter γ, which is involved only in nonlinear terms.

B. Linear instability

We have determined the onset of the longitudinal instability by numerical simulation of a 1D system. The uniform stationary state becomes unstable for $\alpha_0>\alpha_{\|}\simeq 6.16$. The inhomogeneous profile just beyond the transition is given in Fig. 7. The transition does not occur for $\alpha_0=\alpha_c=7.8125$, but is delayed until the width of the supercritical domain is larger than a critical value, here when $\Delta L\approx 0.65\lambda$.

The transverse instability was studied by following the emergence of a pattern in the median plane. We have determined, not only the onset of this instability, but also the dispersion curves $\sigma(\mathbf{k}_\perp)$ (Fig. 8) by following, after the fast relaxation onto the unstable eigenvector, the growth of a small perturbation of wavevector $\mathbf{k}_\perp$ and amplitude A. Since, in the linear regime, the amplitude grows according to the

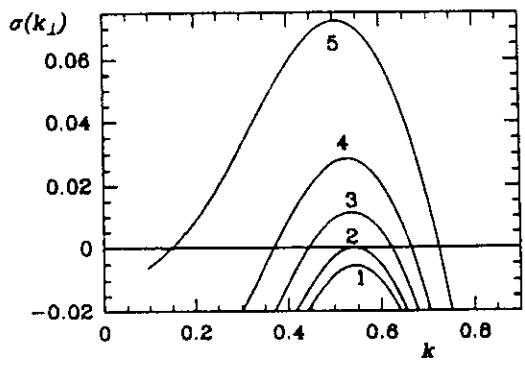

FIG. 8. Dispersion curves: growth rate $\sigma(k_\perp)$ for different α_0 values. (1) $\alpha_0=7.2$, (2) $\alpha_0=7.1350$, (3) $\alpha_0=7$, (4) $\alpha_0=6.8$, (5) $\alpha_0=6.3$.

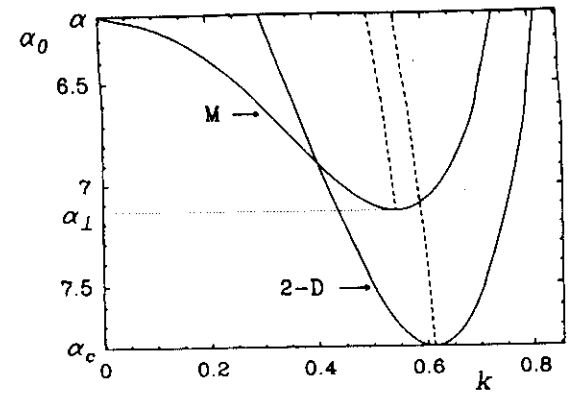

FIG. 9. Marginal stability curves of 2D and monolayer (M) systems. $\sigma(k_\perp)$ is maximal on dotted lines.

equation $dA/dt=\sigma(k_\perp)A$, where $k_\perp=|\mathbf{k}_\perp|$, the eigenvalue σ is constant in time and given by

$$\sigma(k_\perp)=\frac{\ln\left(\dfrac{A(t+\Delta t)}{A(t)}\right)}{\Delta t}. \tag{14}$$

A comparison of the upper and the lower limits of the unstable band as a function of α_0 with those obtained analytically for the genuine 2D systems is given in Fig. 9. The transverse instability is delayed to $\alpha_0=\alpha_\perp\simeq 7.135>\alpha_c$, i.e., $\Delta L\approx 0.41\lambda$. However, since $\alpha_\perp>\alpha_{\|}$, this transverse instability precedes the longitudinal instability, so that the critical value is $\alpha_{0c}=\alpha_\perp$ and $\Delta\alpha_0=\alpha_\perp-\alpha_0$.

A significant feature of the monolayer system is that the sideband rapidly expands on the lower side of $k_\perp$ when the distance $\Delta\alpha_0$ increases. The transverse mode $k_\perp=0$ becomes actually unstable for $\alpha_0=\alpha_{\|}$. Therefore, the longitudinal instability behaves like an homogeneous instability for the structures that develop in the transverse direction. This property will take a major importance in the interpretation of the nonlinear properties in Sec. III C. Another noticeable difference with the genuine 2D case is the shift to lower values of the wave vector corresponding to the maximum growth, i.e., the most unstable mode.

In order to check that the succession of the instabilities does not depend on the choice of the linear coefficient on which the parameter ramp is applied, we have successively applied this ramp to the coefficients α,β or to the coefficients α' and β' which come from a different normalization of the linearised equations:

$$\frac{\partial u}{\partial t}=\alpha' u-v,$$
$$\frac{\partial v}{\partial t}=\beta' u-v. \tag{15}$$

We have kept the parabolic profile but the factor ρ has been adjusted to meet the conditions that define a monolayer system, but, to avoid additional spurious effects, we have required that for the most subcritical values the system do not comes close to an unstationary instability [e.g., when $\beta(z)\sim 0$]. In this purpose the parabolic profile is limited to the central region and limited to a nondangerous constant subcritical value elsewhere (e.g., $\beta=1.5$). These minor

TABLE I. Values of computed critical parameters.

Model	Control parameters	ρ	2D system	Transverse instability (ΔL)	Longitudinal instability (ΔL)
$\begin{pmatrix} 1 & -\alpha \\ 1 & -\beta \end{pmatrix}$	$\beta=5$	0.15	$\alpha_c=7.8125$	$\alpha_\perp=7.135$ (0.41λ)	$\alpha_\parallel=6.16$ (0.65λ)
$\begin{pmatrix} 1 & -\alpha \\ 1 & -\beta \end{pmatrix}$	$\alpha=7$ $\beta\geq 1.4$	−0.15	$\beta_c=3.66$	$\beta_\perp=4.53$ (0.49λ)	$\beta_\parallel=5.77$ (0.76λ)
$\begin{pmatrix} \alpha' & -1 \\ \beta' & -1 \end{pmatrix}$	$\beta'=2$ $\alpha'>0$	−0.012	$\alpha'_c=0.582$	$\alpha'_\perp=0.640$ (0.36λ)	$\alpha'_\parallel=0.783$ (0.67λ)
$\begin{pmatrix} \alpha' & -1 \\ \beta' & -1 \end{pmatrix}$	$\alpha'=0.6$	0.1	$\beta'_c=2.112$	$\beta'_\perp=1.599$ (0.37λ)	$\beta'_\parallel=1.067$ (0.53λ)

changes are always located well outside the core of the monolayer [43] The values of the computed critical parameter are collected in Table I.

Whichever the ramped coefficient is, both instabilities are always delayed and the transverse instability always comes first. This precedence was also predicted some time ago by Dewel *et al.* [20], on the basis of slightly different hypotheses. We shall now focus exclusively on model (3) in the case where the spatial profile is set on parameter α.

C. Stability and pattern selection

To analyze the two-dimensional symmetries of the different monolayer patterns, one can use different concentration amplitudes. Natural choices are the concentrations in the median plane, that is the most supercritical region with the higher contrast, or the spatial average of concentrations over the system depth, i.e., over the range $0<z<L$. The latter representation more closely mimics the experimental observation in the disk reactor. In practice, there is no qualitative differences between these two descriptions, as shown in Fig. 10, where both representations of the same monolayer of hexagonal symmetry are given. To evidence the monolayer character of the structure, a vertical section parallel to $\mathbf{O}_x$ is also shown. Other plane sections parallel to the faces exhibit the same symmetry, so that one can refer to the 2D terminology to classify the monolayers. If not otherwise stated, the reported amplitudes will always correspond to the concentrations in the median plane.

In Fig. 11, the different kinds of monolayer patterns observed in our numerical simulations are collected. They exhibit precisely the same planforms as the genuine 2D systems, that is hexagons H_0 or H_π, and straight or zigzag stripes (compare with Fig. 3).

The bifurcation diagrams for the monolayers at $\gamma=0.75$ are reported in Fig. 12. The wavelength is set to the critical value. Note that, contrary to diagrams of Sec. II, full and dotted lines do not represent analytical predictions, but are

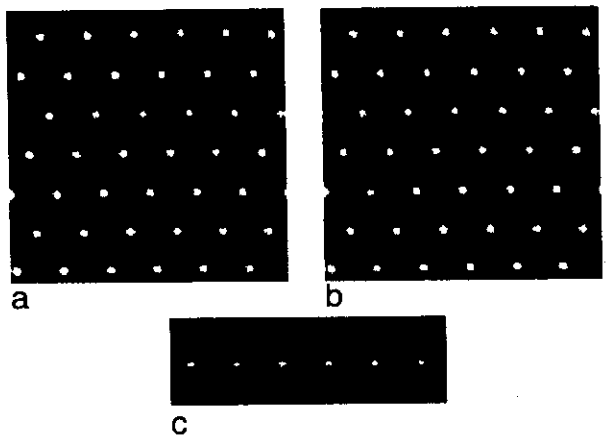

FIG. 10. Monolayer pattern. $\alpha_0=7$, $\rho=0.15$, $\beta=3$, $\gamma=3$, $d=20$, size: 80×80×27. (a) distribution of concentration u in the median plane; (b) distribution of concentration u averaged over the system depth; (c) distribution of concentration u in a plane $(\mathbf{O}_x,\mathbf{O}_z)$ parallel to the parameter gradient.

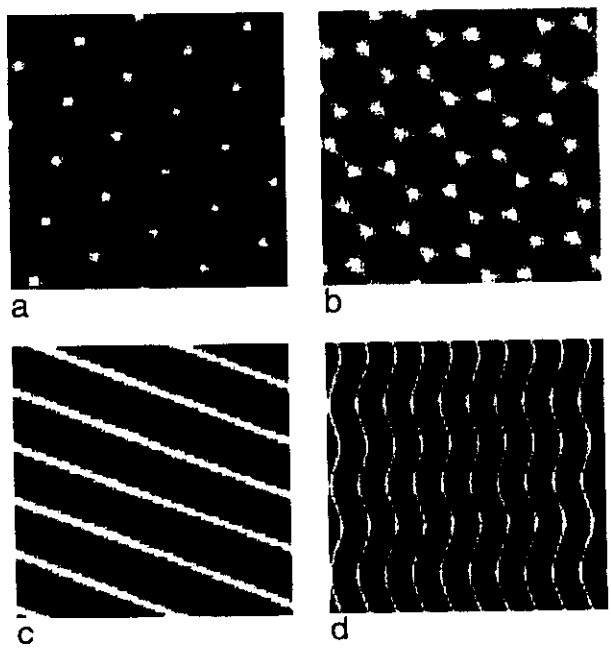

FIG. 11. Monolayer patterns: distribution of concentration u in the median plane. Common parameters: $\rho=0.15$, $\beta=5$, $d=20$. (a) hexagonal pattern H_0 ($\alpha_0=7$, $\gamma=3$, size: 60×60×27); (b) hexagonal pattern H_π ($\alpha_0=7$, $\gamma=-3$, size: 60×60×27); (c) striped pattern ($\alpha_0=7$, $\gamma=0$, size: 60×60×27); (d) zigzag pattern ($\alpha_0=6.6$, $\gamma=3$, size: 127×127×27).

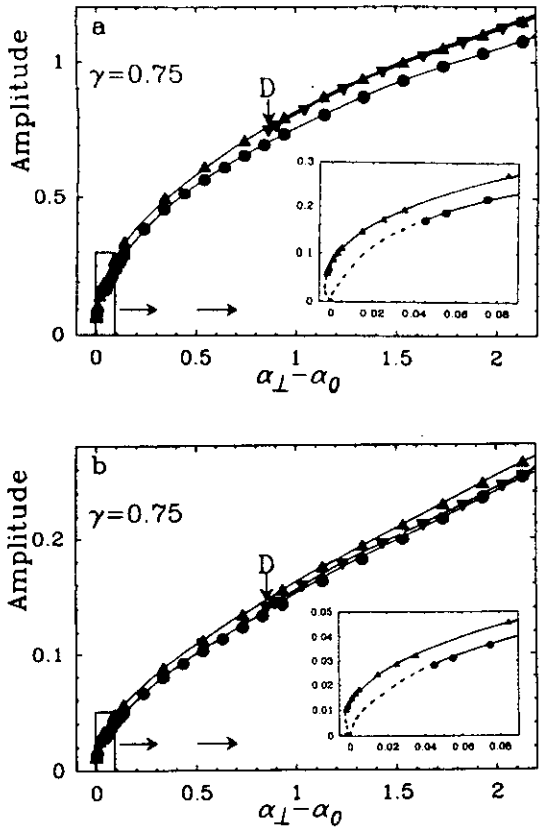

FIG. 12. Bifurcation diagrams for monolayers at $\gamma=0.75$ (amplitude of variable u). $\rho=0.15$, $\beta=5$, $d=20$. ▲: stable hexagons H_0. ▼: stable hexagons H_π (limit at point D). ●: stable stripes. —: stable states. ---: unstable states (numerical simulation). (a) amplitude in the median plane, (b) amplitude averaged over the system depth.

drawn to highlight the continuity of the numerical branches. In Fig. 12(a), we used the amplitude A_{max} in median plane, whereas in Fig. 12(b), we used the amplitude A_{ave} averaged over the system depth. As expected, both diagrams exhibit the same qualitative behavior. Close to onset, they are similar to those of 2D systems. The hexagonal form H_0 bifurcates first in a subcritical way. The stripe pattern branch is supercritical but is unstable nearly beyond onset. It recovers stability at some distance from the bifurcation point.

Close to onset, the amplitude A_{ave} remains finite. This attests that the layer thickness δ does not vanish at the critical point. This thickness can actually been estimated from the values of the maximum and averaged amplitude if one assume that the amplitude of a fully developed structure averaged on a wavelength should be about $A_{max}/2$. In our system, one has $L/\lambda\sim3$. From Figs. 12(a) and 12(b) one gets $A_{max}/A_{ave}\sim6\sim2L/\lambda$ from which we can give an estimated value $\delta\sim2LA_{ave}/A_{max}\sim\lambda$. Therefore, at onset, the layer arises at once with a thickness of one wavelength. When $\gamma\neq0$, this in agreement with the subcritical character of the bifurcation but in contrast with the analog problem in lower dimensions. Actually, in two-dimensional systems where one imposes a gradient of input reactant concentrations, the transition was essentially found to be supercritical [21].

Although, in the close vicinity of the bifurcation point, genuine 2D systems and monolayers exhibit similar stability

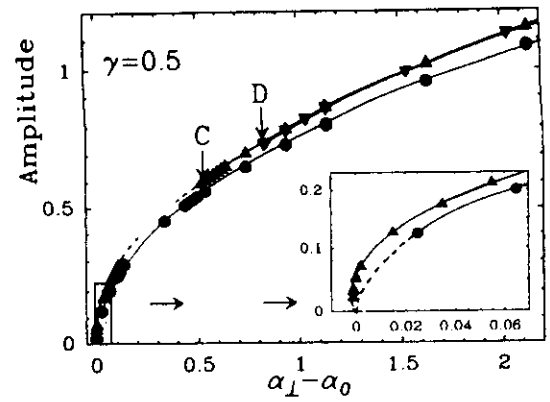

FIG. 13. Bifurcation diagram for the monolayers at $\gamma=0.5$ (amplitude of variable u). $\rho=0.15$, $\beta=5$, $d=20$. ▲: stable hexagons H_0 (limit at point C). ▼: stable hexagons H_π (limit at point D). ●: stable stripes. —: stable states. ---: unstable states (numerical simulation).

properties, in the latter, the hexagonal phase H_0 does not lose stability away from onset. For smaller values of γ, the hexagonal branch loses indeed its stability (see Fig. 13, $\gamma=0.5$), vanishing as expected when $\gamma=0$ (Fig. 14), but retrieves rapidly this stability at larger values of $\Delta\alpha_0$ as shown in Figs. 13 and 14. Whichever the value of γ is, a stable branch of H_π hexagons also comes out at some distance from onset. Contrary to the two dimensional case of Figs. 5, this branch exists at $k=k_c$. When $\gamma=0$, the stability ranges of the branches H_0 and H_π merge. In Fig. 15, we represent the different stability domains as a function both of $\Delta\alpha_0=(\alpha_\perp-\alpha_0)$—the distance to onset—and of the parameter γ. The stability limits are identical for γ and $-\gamma$ except that the hexagon types H_0 and H_π are exchanged.

IV. DISCUSSION AND CONCLUSION

We have shown that close to onset, 2D systems and monolayers have similar stability properties but that in the latter, when the distance to onset increases, both hexagonal phases are strongly restabilised. In the range where stripe patterns are also stable, patterns that form spontaneously from random fluctuations of the uniform state are indeed

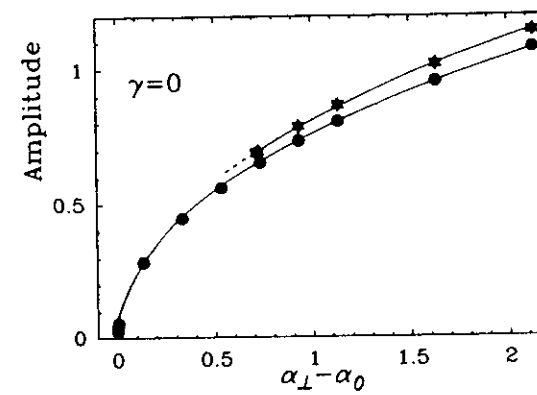

FIG. 14. Bifurcation diagrams for the monolayers at $\gamma=0$, $\rho=0.15$, $\beta=5$, $d=20$. ▲: stable hexagons H_0 and H_π. ●: stable stripes. —: stable states. ---: unstable states (numerical simulation).

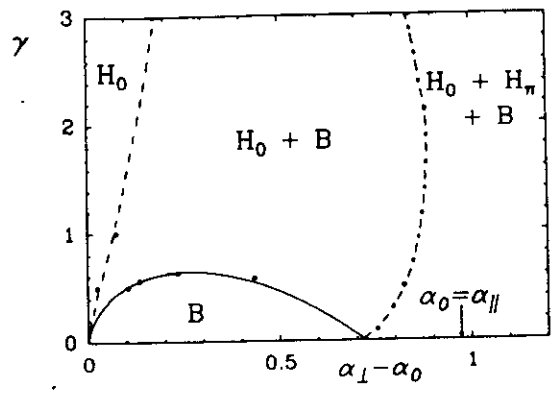

FIG. 15. Nature and stability of patterns in the parameter space (α_0,γ). $\rho=0.15$, $\beta=5$, $d=20$. —: stability limit of hexagons H_0. ----: stability limit of hexagons H_π. ---: stability limit of stripes. H_0, H_π, and B, respectively, specify the stability region of patterns H_0, H_π, and stripes.

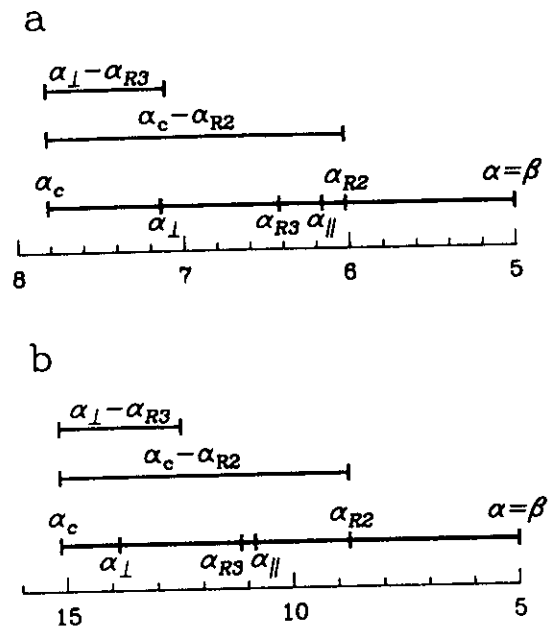

FIG. 16. Summary of relevant stability limits in 2D and monolayer systems. All quantities are defined in the text. (a) $\gamma=0$, $\beta=5$, $d=20$, $\rho=0.15$; (b) $\gamma=0$, $\beta=5$, $d=50$, $\rho=0.25$.

stripes, but this does not dismiss the importance of these hexagonal phases. Since the latter usually bifurcate first, they can be maintained afterwards by a slow continuous change of tunable parameters such as α_0 or γ. This should be a widespread situation in real experiments, where the concentrations gradients build up progressively from the initial state without physical break off. Simultaneous stabilization and/or reentrance of *both* types of hexagonal patterns suggests a d.c. mode induced reentrance. Although we have shown in Sec. II B, that the 2D model exhibits such a phenomenon in relation with a transcritical or pitchfork bifurcation at $\alpha=\beta$, this reentrance has a different origin in the monolayers. Due to the delayed bifurcation, it is more pertinent to use the deviations to onset $\Delta\alpha$ and $\Delta\alpha_0$ than the parameters α and α_0 to compare the stability of the 2D systems and of the monolayers. Accordingly, the restabilization of hexagonal phases turns out to be strongly advanced in the monolayers, as illustrated in Fig. 16(a) in the case $\gamma=0$. This particular example was chosen for simplicity since there is no hexagonal pattern at onset and since H_0 and H_π are both reentrant at the same value $\alpha=\alpha_{R3}$. The shift suggests that the origin of the d.c. mode is different in the two types of systems. Moreover, α_{R3} is close to $\alpha_\parallel$, the value at which the longitudinal instability occurs. To corroborate this point, the numerical simulations have been repeated with $d=50$ [Fig. 16(b)]. In the monolayers the restabilization point is again significantly advanced, but remains still located nearby the longitudinal instability. As we have shown in Sec. II B, this instability actually behaves like a homogeneous instability (d.c. mode) for the transverse structures of wave vector $k_\perp$. It is thus natural that the coupling with this mode restabilizes these transverse hexagonal structures that constitute the monolayer, in agreement with the Price theory. Therefore, the origin of the d.c. mode is quite different in the genuine 2D systems and in the monolayers. In the former, it resulted from the specific form of the reactive part (and could be absent in other models), whereas, in the latter, it follows from the "geometric" effect induced by the concentrations gradients that confine the structure. It is an intrinsic property of these monolayers.

So far, we have used a control parameter profile symmetric with respect to the plane $z=\frac{1}{2}L$. However, we have checked that the properties reported above do not depend on this particular choice by replacing the symmetric parabola by two half-parabolas with different curvatures [30]. The results are definitely similar to those of Sec. III and are not reported here.

In conclusion, we have shown than monolayer Turing patterns arise from a transverse instability with a delay when compared to the genuine 2D systems. The first pattern develops over a full wavelength in the direction $\mathbf{O_z}$. Very close to onset, monolayers and 2D patterns exhibit similar stability properties, but important changes occur in the vicinity of the longitudinal instability: the dispersion curve stretches toward a d.c. mode and, consequently, both hexagonal patterns H_0 and H_π are (re)stabilized. Thus, one can say that the patterns lose their two-dimensional character close to this longitudinal instability. Nevertheless, this instability does not correspond to any visual qualitative change of the structure—visible multiple layers actually come far beyond the transition—so that it seems experimentally impossible to distinguish the narrow parameter range where the 2D description is valid from that of the ambiguous—between 2D and 3D—regime that comes next. Thus, contrary to what is commonly accepted, one should be very cautious in the application of the well developed 2D pattern selection formalism to the experimental results, even when the structure is restricted to a single layer.

ACKNOWLEDGMENTS

We greatly acknowledge P. De Kepper for a critical reading of the manuscript and E. Dulos, P. Borckmans, G. Dewel, A. De Wit, and C. Price for numerous fruitful discussions. This work has been supported by the European Community Science program (Contract No. SC1-CT91-0706).

[1] G. Nicolis and I. Prigogine, *Self-organization in Nonequilibrium Chemical Systems* (Wiley, New York, 1977).
[2] H. Haken, *Synergetics, an Introduction* (Springer-Verlag, Berlin, 1977).
[3] R. J. Field and M. Burger, *Oscillations and Traveling Waves in Chemical Systems* (Wiley, New York, 1985).
[4] J. D. Murray, *Mathematical Biology* (Springer-Verlag, Berlin, 1989).
[5] A. S. Mikhailov, *Foundations of Synergetics I* (Springer-Verlag, Berlin, 1990); A. S. Mikhailov and A. Y. Loskutov, *Foundations of Synergetics II* (Springer-Verlag, Berlin, 1991).
[6] A. M. Turing, Philos. Trans. R. Soc. London B **327**, 37 (1952).
[7] R. Kapral and K. Showalter, *Chemical Patterns and Waves* (Kluwer, Amsterdam, 1995). This reference contains several feature articles on Turing patterns.
[8] P. De Kepper, J. Boissonade, and I. Epstein, J. Phys. Chem. **94**, 6525 (1990).
[9] V. Castets, E. Dulos, J. Boissonade, and P. De Kepper, Phys. Rev. Lett. **64**, 2953 (1990).
[10] P. De Kepper, V. Castets, E. Dulos, and J. Boissonade, Physica D **49**, 161 (1991).
[11] J. Boissonade, in *Bifurcation and Chaos: Analysis, Algorithms, Applications*, edited by R. Seydel, F. W. Schneider, T. Küpper, and H. Troger, Int. Ser. Num. Math. Vol. 97 (Birkhäuser, Basel, 1991), p. 67.
[12] Q. Ouyang and H. L. Swinney, Nature **352**, 610 (1991).
[13] Q. Ouyang and H. L. Swinney, Chaos **1**, 411 (1991).
[14] I. Lengyel, S. Kádár, and I. Epstein, Phys. Rev. Lett. **69**, 2729 (1992).
[15] Q. Ouyang, Z. Noszticzius, and H. L. Swinney, J. Phys. Chem. **96**, 6773 (1992).
[16] J. Boissonade, E. Dulos, and P. De Kepper, in *Chemical Patterns and Waves* (Ref. [7]), p. 221.
[17] M. Herschkowitz-Kaufman and G. Nicolis, J. Chem. Phys. **56**, 1890 (1972).
[18] J. F. Auchmuty and G. Nicolis, Bull. Math. Biol. **37**, 323 (1975).
[19] L. Kramer, E. Ben-Jacob, H. Brand, and M. C. Cross, Phys. Rev. Lett. **49**, 1891 (1982).
[20] G. Dewel, D. Walgraef, and P. Borckmans, J. Chim. Phys. (France) **84**, 1335 (1987).
[21] J. Boissonade, J. Phys. (France) **49**, 541 (1988).
[22] G. Dewel and P. Borckmans, Phys. Lett. **138**, 189 (1989).
[23] A. De Wit, P. Borckmans, and G. Dewel, in *Instabilities and Nonequilibrium Structures IV*, edited by E. Tirapegui and W Zeller (Kluwer, Amsterdam, 1993).
[24] B. A. Malomed and A. A. Nepomnyaschy, Europhys. Lett. **21**, 195 (1993).
[25] B. A. Malomed, Phys. Rev. E **47**, R2257 (1993).
[26] P. Borckmans, G. Dewel, A. De Wit, and D. Walgraef, in *Chemical Patterns and Waves* (Ref. [7]).
[27] A. De Wit, Ph.D. Thesis, U.L.B., Brussels, 1994.
[28] C. Price, Phys. Lett. A **194**, 385 (1994); G. Dewel, S. Metens, M'F. Hilali, P. Borckmans, and C. B. Price, Phys. Rev. Lett. **74**, 4647 (1995).
[29] A. R. Gourlay, J. Inst. Math. Appl. **6**, 375 (1970); A. R. Gourlay and G. R. McGuire, *ibid.* **7**, 216 (1971).
[30] V. Dufiet, Ph.D. Thesis, Univ. of Bordeaux, 1994.
[31] H. Fujii H., M. Mimura, and Y. Nishiura, Physica D **5**, 1 (1982).
[32] A. Hunding, Physica A **188**, 172 (1992).
[33] P. Manneville, *Dissipative Structures and Weak Turbulence* (Academic, New York, 1990).
[34] H. Sakagushi, Prog. Theor. Phys. **86**, 759 (1991); S. Sasa, *ibid.* **84**, 1009 (1990).
[35] V. Dufiet and J. Boissonade, J. Chem. Phys. **96**, 664 (1991).
[36] V. Dufiet and J. Boissonade, Physica A **188**, 158 (1992).
[37] J. Verdasca, A. De Wit, G. Dewel, and P. Borckmans, Phys. Lett. A **168**, 194 (1992).
[38] L. M. Pismen, in *Dynamics of Nonlinear Systems*, edited by V. Hlavacec (Gordon and Breach, New York, 1986), p. 47.
[39] F. H. Busse, J. Fluid Mech. **30**, 625 (1967).
[40] S. Ciliberto, P. Coullet, J. Lega, E. Pampaloni, and C. Perez-Garcia, Phys. Rev. Lett. **65**, 2370 (1990).
[41] In Rayleigh-Bénard convection, this quadratic term is related to the non-Boussinesq effects and normally appears as a small correction.
[42] I. Lengyel and I. R. Epstein, Science **251**, 650 (1991); I. Lengyel, S. Kadar, and I. R. Epstein, *ibid.* **259**, 493 (1993); I. Lengyel and I. R. Epstein, in *Chemical Patterns and Waves* (Ref. [7]), p. 297.
[43] This technical trick could be avoided by using a bomed spatial profile such as a Gaussian, but the number of free parameters would increase.